International Journal of Scientific Interdisciplinary Research

Volume: 1; **Issue:** 1
Pages: 129– 162

CFD-BASED INVESTIGATION OF HEAT TRANSFER EFFICIENCY IN RENEWABLE ENERGY SYSTEMS

Saikat Sarkar[1];

[1]. *Master of Engineering in Mechanical Engineering (Continuing), Lamar University, Texas, USA; Email: saikat.mac@gmail.com*

Doi: 10.63125/ttw40456

Received: *12 October 2021;* ***Revised:*** *20 November 2022;* ***Accepted:*** *18 December 2021;* ***Published:*** *12 January 2022*

Abstract

This study addresses a persistent problem in renewable-energy subsystems: designers often report heat-transfer gains without fairly accounting for hydraulic penalties, which leads to weak deployment decisions. The purpose was to quantify heat-transfer efficiency using an energy-fair metric and test whether documented gains align with practitioner willingness to adopt. The international energy transition emphasizes reductions in thermal losses and improvements in thermo-hydraulic performance across solar thermal collectors, geothermal borehole heat exchangers (BHEs), and thermal energy storage (TES) modules.Well-constructed CFD provides a "virtual laboratory" to explore feasible designs over realistic operating ranges without incurring prohibitive prototyping or test-rig costs, while still supporting validation against standard correlations and selected experiments. This study used a quantitative, cross-sectional, case-based design integrating validated CFD outputs with a Likert five-point practitioner survey. The sample comprised two technology cases, a rib-augmented solar thermal channel and a coaxial deep borehole heat exchanger, with DOE-style CFD sweeps producing 312 runs and a practitioner sample of 184 responses. Key variables were area-averaged Nusselt number, pressure drop, a thermal-efficiency proxy, and the equal-pumping-power performance evaluation criterion (PEC); predictors included Reynolds number, standardized geometry indices, and their interaction. The analysis plan specified descriptive statistics, HC3-robust regressions with case fixed effects, marginal effects, and subgroup checks, with mesh independence verified at <2 percent drift and heat-balance error ≤0.5 percent. Headline findings show PEC averaged 1.08±0.09, with PEC ≥1.10 concentrated at mid to high Reynolds and moderate geometry; ln(Re) and geometry had positive effects on Nu and PEC, including a significant interaction. Survey constructs were reliable (Cronbach's a ≥0.80). Perceived efficiency averaged about 4.0 on a five-point scale and correlated with standardized PEC (r≈+0.56), while adoption intention rose from 3.36 in the lowest PEC quartile to 4.18 in the highest. Implications are clear: institutionalize equal-constraint reporting, target moderate augmentation at mid to high Reynolds to maximize PEC beyond 1.10, and couple design with light O&M monitoring to sustain realized gains.

Keywords

Computational fluid dynamics (CFD), Performance evaluation criterion (PEC), Heat-transfer efficiency, Reynolds number, Nusselt number.

INTRODUCTION

Computational Fluid Dynamics (CFD) is the numerical solution of the conservation equations of mass, momentum, and energy to predict transport behavior velocity, pressure, temperature, and scalar fields in complex domains under specified boundary conditions. Within renewable energy systems, CFD enables the quantification of local convective and conductive mechanisms that govern collector, exchanger, and storage performance, thereby revealing how geometry, material properties, and operating set-points shape heat transfer efficiency, which can be defined as the effectiveness with which an available thermal potential is converted into useful heat delivery to a working fluid (Bhushan & Singh, 2012). The international energy transition emphasizes reductions in thermal losses and improvements in thermo-hydraulic performance across solar thermal collectors, geothermal borehole heat exchangers (BHEs), and thermal energy storage (TES) modules.Well-constructed CFD provides a “virtual laboratory” to explore feasible designs over realistic operating ranges without incurring prohibitive prototyping or test-rig costs, while still supporting validation against standard correlations and selected experiments (Celik et al., 2008). In solar thermal technologies, boundary-layer manipulation over absorber plates and riser channels controls local Nusselt number distributions, with the attendant pumping-power penalties captured by friction factors that CFD resolves with near-wall modeling (Fan et al., 2009). In geothermal DBHE systems, coupled models of internal convection and subsurface conduction characterize sustainable extraction over seasonal cycles and deeper time horizons (Le Lous et al., 2015; Sanjid & Farabe, 2021). In TES based on phase-change materials (PCMs), enthalpy–porosity formulations capture moving solid–liquid fronts, allowing systematic study of fins, foams, and multi-tube layouts for faster charge/discharge while preserving storage capacity (Agyenim et al., 2010; Le Lous et al., 2015). Across these domains, the international significance of heat transfer efficiency is anchored in reliable, validated, and reproducible modeling that links local transport phenomena to system-level performance indicators using metrics such as the performance evaluation criterion (PEC) and energy-saving oriented comparison plots (Fan et al., 2009).

Figure 1: 3D Representation of Computational Fluid Dynamics (CFD) Applications in Renewable Energy Systems

At the device scale, solar air and liquid collectors illustrate the central thermo-hydraulic trade-off: geometric augmentation enhances heat transfer by disrupting the viscous sublayer and intensifying mixing, while increasing flow resistance that raises auxiliary energy demand. The “performance evaluation plot” framework consolidates this comparison by viewing enhancement and penalty together under equal flow, equal pressure drop, or equal pumping-power constraints, thereby orienting decisions toward energy saving rather than raw heat transfer gains (Hans et al., 2009). Empirical–CFD programs have tested and simulated artificial roughness geometries arc-shaped wires, ribs, and protrusions to develop correlations for Nusselt number and friction factor over ranges of roughness height, relative pitch, angle, and Reynolds number, supplying a compact mapping between design variables and outcomes (Zaman & Momena, 2021; Saini & Saini, 2008). CFD's strength here lies in near-wall resolution and turbulence modeling that reproduce separation and reattachment sequences responsible for augmentation, while mesh independence checks and residual-based convergence criteria stabilize the numerical predictions used in regression or surrogate modeling (Celik et al., 2008; Rony, 2021). In addition, studies of rib orientation, dimple-rib combinations, and compound enhancements in rectangular or trapezoidal ducts report meaningful gains in average Nusselt numbers and PEC values when geometry is tuned within bounded ranges, a finding that emerges consistently across numerical and experimental approaches (Hosseinizadeh et al., 2005; Sudipto & Mesbaul, 2021). This body of evidence positions CFD not only as a design-screening tool but also as a bridge to generalizable statistical models linking Reynolds number, geometric encodings, and mass-flow selection to heat transfer efficiency suitable for cross-case comparisons presented later in quantitative sections of such studies (Fan et al., 2009; Zaki, 2021).

Figure 2: Coupled Convection–Conduction Processes and Thermal Resistance Network in a Coaxial DBHE System

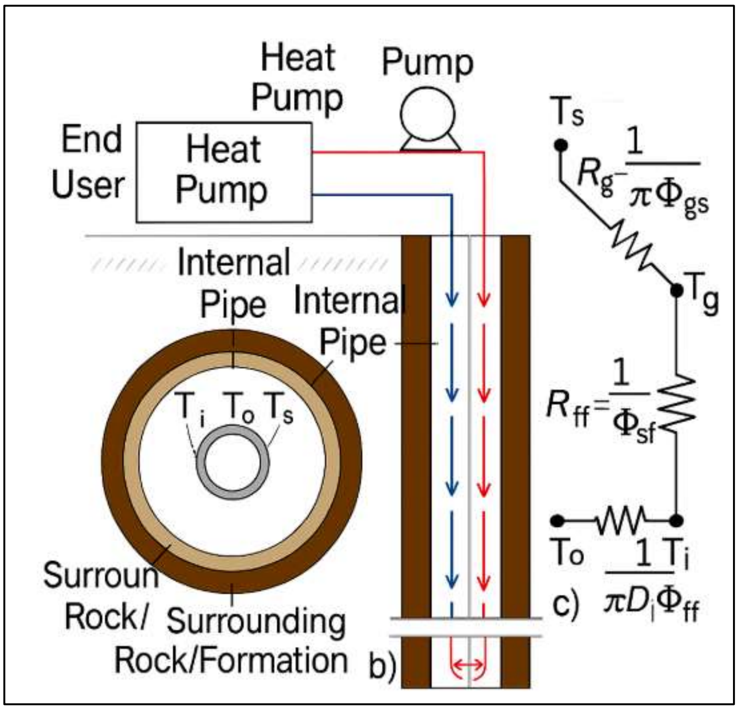

Geothermal DBHEs represent a complementary context where heat transfer efficiency is shaped by a coupled system: internal convection through a coaxial or U-tube assembly interacts with axial conduction and radial heat flow into the rock mass. Synthetic and site-calibrated studies have used three-dimensional CFD or hybrid numerical models to analyze the effects of borehole diameter, flow regime, inlet temperature, and rock thermal properties on long-term extraction, outlet temperature stability, and drawdown (Congedo et al., 2012; Hozyfa, 2022). Design variables such as annulus thickness, insulation between strings, and inlet–outlet configuration govern short-circuiting and thermal breakthrough, while operational variables such as mass flow rate and cycling schedules set sustainable capacity, all of which are accessible to parametric sweeps coupled with verification steps (Cabeza et al., 2011; Arman & Kamrul, 2022). The literature demonstrates how combined conduction–convection formulations replicate measured temperature histories and thermal response tests when material properties and boundary conditions are specified carefully, supporting the selection of practical KPIs such as specific extraction per meter and seasonal coefficient of performance (Li & Lai, 2012; Mohaiminul & Muzahidul, 2022). In this context, CFD offers detailed resolution of internal flow fields (including secondary flows at bends or in the annulus) and wall heat fluxes, while the geological domain is handled through validated conduction models that incorporate far-field boundary conditions and vertical gradients. The assembled results characterize how design and operation influence heat transfer efficiency and pumping power in a manner consistent with broader renewable system goals, with reproducibility anchored by grid-refinement studies and documented solver settings (Omar & Ibne, 2022; Medrano et al., 2010).

In TES modules employing PCMs, the working concept is the absorption or release of latent heat during phase change within a designated temperature window. Heat transfer efficiency depends on how quickly and uniformly the module melts or solidifies while maintaining acceptable pressure drops and exergy losses across the connected hydraulic loop. CFD models relying on enthalpy–porosity or effective property methods capture moving phase interfaces and buoyancy-driven convection in the melt, enabling quantitative assessment of fin geometries, metal foams, and multi-tube configurations (Agyenim et al., 2010; Sanjid & Zayadul, 2022). Experimental and numerical studies have shown that conductive pathways through fins and high-porosity foams intensify heat transfer, reduce charging times, and improve spatial uniformity of temperature, with model–experiment agreement established through temperature histories and liquid fraction tracking (Al-Abidi et al., 2013; Hasan, 2022). Earlier numerical work on unconstrained melting and enclosure effects established the sensitivity of melt patterns to Rayleigh number, enclosure aspect ratio, and boundary heating, reinforcing the importance of mesh strategies and temporal accuracy in CFD predictions used for design (Bergles, 2012; Mominul et al., 2022). Review articles further consolidate materials and modeling practice, highlighting the role of property data quality, formulation choices, and validation protocols in ensuring credible comparisons across studies (Eça & Hoekstra, 2008; Rabiul & Praveen, 2022). These contributions frame the statistical modeling of CFD-derived outcomes charge/discharge time, outlet temperature trajectories, and PEC analogs for storage within a coherent evidence base suitable for regression, correlation, and subgroup analyses.

Heat-transfer-dominated internal flows are often turbulent with separation and reattachment near augmented surfaces; therefore, turbulence closure and near-wall treatment influence predicted wall heat fluxes and friction factors. The SST k–ω framework blends near-wall accuracy with free-stream robustness, providing credible predictions for adverse-pressure-gradient and impingement-like regions frequently encountered in enhanced ducts and headers (Chamoli, 2013; Farabe, 2022). Sensitivity studies demonstrate that quantitative outputs for Nusselt number and pressure drop respond to closure choices and discretization settings, motivating standardized verification procedures (Hans et al., 2009; Roy, 2022). Grid convergence indicators, residual reduction targets, and heat-balance closure checks help distinguish numerical artifacts from genuine design effects, thereby legitimizing the use of CFD outputs in statistical generalization steps such as linear models with interaction terms and case fixed effects. In augmented channels and PCM enclosures, careful control of near-wall y^+, inflation layers, and second-order spatial schemes supports the stability and reproducibility necessary for cross-study synthesis (Khodadadi & Hosseinizadeh, 2007; Rahman & Abdul, 2022). In BHE simulations, grid and time-step sensitivity are coupled with domain-size checks to ensure that far-field thermal boundaries do not spuriously constrain predicted extraction (Liang et al., 2018; Razia, 2022). Collectively, these verification practices underwrite the quantitative claims reported in energy-systems CFD and provide a methodological foundation for constructing regression-ready datasets from design-of-experiments (DOE) sweeps across geometry and flow variables (Promvonge, 2008; Zaki, 2022).

Enhanced heat transfer strategies are routinely categorized as passive (geometry, surface texturing, foams) and active (moving inserts, pulsation), with energy-systems applications favoring passive concepts due to reliability and ease of integration. Reviews of enhanced techniques emphasize that performance must be framed in energy-saving terms rather than raw heat transfer increases, aligning comparisons through unified metrics such as PEC and energy-based criteria under constraint matching (Signorelli et al., 2005). In solar air heaters, triangular, arc-shaped, V-shaped, and dimple-rib patterns have been evaluated across Reynolds number regimes with empirical correlations supported by CFD flow visualization and wall shear distributions (Scarpa et al., 2014; Kanti & Shaikat, 2022). In PCM modules, morphological features like fin spacing and foam porosity control effective conductivity and melt front topology, producing systematic effects in charge/discharge times documented through coupled experiment–CFD workflows (Tyagi & Buddhi, 2007). In geothermal DBHEs, internal configuration and insulation schemes adjust thermal short-circuiting in the annulus, with numerical studies mapping combinations that protect outlet temperature while maintaining feasible pumping power (Zanchini & Lazzari, 2014). The cross-domain consistency of these findings provides a basis for pooled modeling in quantitative research designs where case dummies, interaction terms, and robustness checks test whether design effects generalize across renewable subsystems (Youssef et al., 2017).

The quantitative, cross-sectional, case-study–based design integrates CFD simulation outputs with survey evidence from practitioners to characterize heat transfer efficiency in renewable subsystems using consistent, reproducible metrics. CFD yields area-averaged Nusselt numbers, thermal efficiency proxies, pressure drops, and energy-oriented performance indices under documented boundary conditions and solver settings; DOE-style sweeps facilitate regression modeling with main effects and interactions for Reynolds number, mass flow rate, and geometric encodings (Jegadheeswaran & Pohekar, 2009). In parallel, a Likert five-point survey captures perceived efficiency gains, implementation complexity, O&M burden, safety, cost-effectiveness, and adoption intention across professional roles in solar, geothermal, and storage contexts, enabling correlation analysis with normalized CFD indicators (Karwa & Chitoshiya, 2013). The literature summarized above provides validated modeling approaches (enthalpy–porosity for PCM, SST k–ω for internal turbulent flows, coupled conduction–convection for DBHEs), verification protocols (grid convergence, residual targets, heat-balance closure), and performance metrics (PEC and thermo-hydraulic criteria) that support coherent measurement of efficiency within and across cases (Celik et al., 2008; Al Amin, 2022). This framing positions the statistical analysis plan descriptive statistics, correlation, and regression with diagnostics as a natural extension of evidence in the field and establishes the foundation for the subsequent sections on methods and results in studies of this kind (Scarpa et al., 2014).

The overarching objective of this study is to quantify heat transfer efficiency in representative renewable energy subsystems using a rigorously specified CFD-and-survey framework, and to express that efficiency in reproducible thermo-hydraulic metrics suitable for statistical modeling. Specifically, the study aims to: (1) establish validated CFD baselines for at least two case-study configurations an augmented solar thermal channel and a deep borehole heat exchanger under clearly defined boundary conditions, turbulence closure, and mesh-independence criteria; (2) execute a structured design-of-experiments across Reynolds number, mass flow rate, and geometry encodings to generate a simulation dataset containing area-averaged Nusselt number, thermal efficiency proxies, pressure drop, outlet temperature, charge/discharge time where applicable, and performance evaluation criteria under matched constraints; (3) estimate and compare regression models that relate thermal outcomes to design and operating variables, including interaction terms and case fixed effects, with diagnostics for multicollinearity, heteroskedasticity, residual normality, and influence; (4) compute marginal effects and response surfaces to characterize practical trade-offs between augmentation and hydraulic cost across the explored factor space; (5) design and administer a Likert five-point survey instrument to practitioners in solar, geothermal, and storage contexts to obtain construct scores for perceived efficiency gains, implementation complexity, operation and maintenance burden, safety, cost-effectiveness, and adoption intention; (6) assess reliability and factor structure of the survey instrument and derive composite indices for subsequent analysis; (7) correlate and regress practitioner constructs on normalized CFD metrics to test alignment or misalignment between modeled performance and professional judgment; (8) perform subgroup and sensitivity analyses by technology type, geometry family, turbulence model choice, and mesh density to evaluate robustness of estimated effects; and (9) summarize the quantitative findings as case-anchored, statistically supported relationships that can be read directly alongside the CFD verification record. By structuring the investigation around these objectives, the study provides a transparent path from physical modeling to statistical inference, ensuring that every reported effect size, comparison, and conclusion rests on a traceable chain of definitions, measurements, and tests consistent with the declared cross-sectional, case-study–based design.

LITERATURE REVIEW

The literature on heat transfer efficiency in renewable energy systems converges on a common premise: device-level transport processes convection, conduction, radiation, and, where relevant, phase change govern system-level performance, and careful modeling of these processes is essential for credible design guidance. Foundational work in solar thermal channels shows how manipulating near-wall behavior through surface geometry, flow conditioning, and material selection can elevate local and average heat transfer while simultaneously affecting hydraulic losses; these thermo-hydraulic trade-offs motivate unified metrics that compare enhancement techniques under matched constraints and not merely under identical flow rates. Parallel developments in geothermal deep borehole heat exchangers emphasize coupled internal–external domains, where conduit convection interacts with rock conduction and groundwater influences to determine sustainable extraction and outlet temperature stability; here, numerical treatments must reconcile internal turbulence resolution with geologic boundary prescriptions. Thermal energy storage based on phase-change materials adds a distinct layer, as latent heat utilization hinges on advancing melt/solidification fronts within typically low-conductivity media; finned structures, porous matrices, and multi-tube layouts are repeatedly examined to accelerate charge/discharge without degrading usable capacity. Across these domains, computational fluid dynamics (CFD) has matured from proof-of-concept simulations to verification-aware studies that report grid independence, turbulence-model sensitivity, and heat-balance closure, enabling results to support statistical generalization rather than isolated case narration. This methodological sharpening aligns with a broader shift from single-metric reporting (e.g., only Nusselt number) toward energy-oriented criteria that integrate pumping power, pressure drop, and thermal effectiveness, making findings more actionable for design and operations. Complementing the modeling stream, practitioner-focused surveys and case protocols increasingly appear in the literature to capture feasibility, maintainability, cost–benefit perception, and adoption intention constructs that determine whether modeled gains translate into deployed improvements. Yet, despite the diversity of technologies and enhancement strategies, a unifying structure emerges: define clear outcome measures, map them to controllable design and operating variables, verify numerical fidelity, and synthesize results through regression or correlation frameworks that can test consistency across cases and subgroups. This review adopts that structure to situate the present study within three focal arenas solar thermal channels, geothermal borehole exchangers, and phase-change storage while foregrounding the verification practices, performance metrics, and statistical modeling choices that convert CFD insights into reproducible, decision-relevant evidence.

Heat transfer in renewable-energy subsystems

Heat transfer processes govern the useful-energy yield, stability, and economic feasibility of most renewable-energy subsystems, from solar thermal collectors to geothermal exchangers and latent-heat storage. In solar air-heater (SAH) ducts, for example, the inherently low air-side heat-transfer coefficient limits thermal efficiency unless convective augmentation is introduced. A mature body of work shows that engineered surface features (rib-roughness, vortex generators, wire coils, and baffles) intensify turbulence in the near-wall region, elevate Nusselt numbers, and thereby lift thermal effectiveness albeit with a hydraulic penalty that must be balanced via thermo-hydraulic performance criteria. A recent synthesis of artificial-roughness geometries details how rib pitch, relative roughness height, and attack angle interact with Reynolds number to control recirculation and reattachment, offering design maps that translate fluid-mechanics insight into higher collector efficiencies in practice (Singh & Singh, 2018). At the subsystem level, flat-plate solar collectors (FPSC) confront additional loss channels optical (reflection), top and edge heat losses, and absorber/back losses which couple with internal convection to shape the useful heat gain. A focused review of FPSC development charts multiple pathways for efficiency gains selective coatings, micro-/mini-channels, absorber geometry optimization, nanofluid working media, and PCM-backed plates each of which hinges on more favorable heat-transfer pathways and reduced thermal resistances (Pandey & Chaurasiya, 2017). Together, this evidence situates convective augmentation and conductive-path engineering as the principal levers for raising solar-thermal subsystem performance under constrained collector area and pumping power.

Figure 2: Heat Transfer Pathways in Renewable-Energy Subsystems

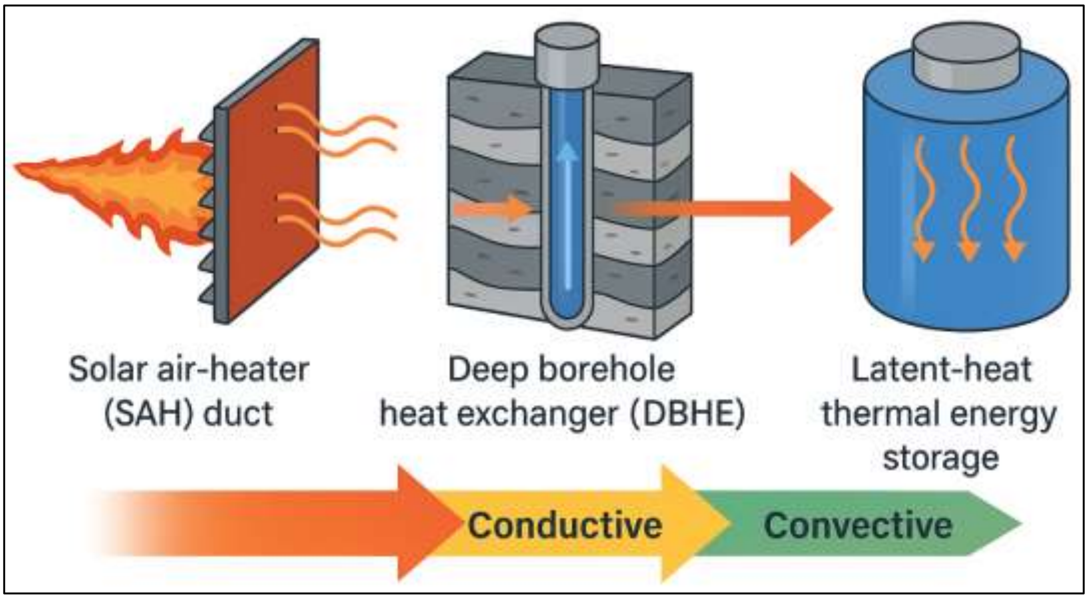

Beyond low-temperature solar subsystems, deep-geothermal heat extraction exemplifies the centrality of conjugate heat transfer (fluid–solid–rock) to system viability. Closed-loop deep borehole heat exchangers (DBHEs) eliminate formation fluid exchange yet rely entirely on axial and radial heat conduction through stratified geological media and forced convection inside the coaxial (or U-tube) borehole circuit. High-fidelity CFD and finite-volume simulations reveal that outlet temperature and heat-extraction rate depend nonlinearly on borehole depth, imposed mass flow, inner-pipe insulation, and local geothermal gradient. In DBHEs deployed in high-gradient systems (e.g., volcanic regions), properly insulated inner strings and optimized flow rates maintain favorable temperature lift while avoiding excessive pumping power or thermal short-circuiting between annulus and inner pipe (Renaud et al., 2019). These models show that the characteristic thermal time constants are long, so parametric choices (pipe diameters, materials, and flow regimes) have multi-year consequences for delivered thermal power. When viewed through a common lens with solar collectors, the same design grammar emerges: maximize the effective heat-transfer area and conductivity on the source side, preserve temperature driving potentials along the fluid pathway, and minimize parasitic hydraulic losses guidelines that are tractable precisely because they rest on transport-phenomena fundamentals (Battula & Bhattacharya, 2019).

Thermal-energy storage (TES), particularly latent-heat systems based on phase-change materials (PCMs), provides the third pillar linking heat-transfer science to renewable-system efficacy. Classic reviews established the rationale for PCMs high volumetric energy density and quasi-isothermal charging/discharging and cataloged materials and encapsulation strategies suitable for solar and efficiency applications (Sharma et al., 2009). The performance bottleneck, however, is the low thermal conductivity of many PCMs, which throttles melting/solidification fronts unless the designer purposefully reshapes conduction and natural-convection pathways. Contemporary CFD studies that resolve finned-tube geometries and porous-metal inserts show that carefully tuned fin shapes, spacing, and placements as well as metal-foam skeletons at appropriate pore densities shorten charging times, smooth temperature fields, and increase effective power without prohibitive mass or cost (Battula & Bhattacharya, 2019). Within solar-thermal assemblies, these enhancements complement the collector-side measures discussed earlier: a PCM-backed FPSC with optimized absorber geometry couples higher solar gain to faster storage kinetics, yielding a flatter and more dispatchable thermal output profile (Pandey & Chaurasiya, 2017). Across these domains, the unifying role of heat-transfer augmentation geometric tailoring for convection and conduction, property management via materials selection, and system-level balancing of thermal and hydraulic metrics provides the conceptual substrate for CFD-driven investigations in this study.

CFD Methods for Conjugate and Turbulent Heat Transfer

Accurate prediction of heat-transfer efficiency in renewable subsystems depends on turbulence closure choices and on how the solid and fluid domains are coupled within a single numerical framework. In most engineering operating ranges, designers begin with Reynolds-Averaged Navier–Stokes (RANS) formulations because they provide stable, affordable predictions across broad parametric sweeps while retaining essential near-wall physics needed for wall heat-flux estimation. Among these, modern variants of the k–ω family remain central because they blend good near-wall behavior with robustness in free shear regions; revisions to dissipation and cross-diffusion terms improved sensitivity to adverse-pressure gradients and separation, which are common in ribbed or baffled channels and in collector headers and risers (Wilcox, 2008). RANS alone, however, is only part of the story for heat-transfer-dominated equipment. Conjugate heat transfer requires simultaneous solution of the energy equation in both fluid and solid regions, enforcing continuity of temperature and normal heat flux at interfaces while the momentum equations govern fluid motion. Numerical stability here depends on mesh compatibility or conservative interpolation across non-conformal interfaces and on consistent temporal treatment when transient charging or drawdown is examined, such as in thermal storage modules or in components that experience cycling. Radiation modeling can further influence predicted wall temperatures and losses in solar subsystems; while discrete ordinates or P-1 approximations are often used, their inclusion increases coupling stiffness and amplifies the need for careful linearization. The combination of RANS closure, conjugate coupling, and radiative transfer thus forms a practical baseline that can support extensive design-of-experiments studies without sacrificing the fidelity required to calculate metrics like Nusselt number, pressure drop, thermal efficiency, and energy-oriented performance evaluation criteria (Wilcox, 2008).

Transition from laminar or weakly turbulent inflow to fully turbulent boundary layers frequently controls local heat-transfer coefficients in renewable hardware, especially where Reynolds numbers hover near regime boundaries or where surface texturing induces intermittent separation. Capturing this behavior has spurred the adoption of correlation-based transition frameworks in general purpose CFD solvers, which augment the transport equations with additional variables that represent intermittency and momentum-thickness Reynolds number. These models are designed to trigger transition based on local freestream turbulence, pressure gradients, and surface roughness surrogates, thereby improving predictions of skin friction and heat transfer on smooth or moderately augmented surfaces without the expense of scale-resolving simulations (Langtry & Menter, 2009). For components with strong three-dimensional separation collector manifolds with sharp turns, vortex-generator fields in air heaters, or complex inlet geometries in borehole heat-exchanger strings hybrid approaches that blend RANS in boundary layers with large-eddy simulation (LES) away from walls can recover unsteady mixing and large coherent structures that drive scalar transport. A well-known development in this direction delays the switch to the LES branch until the grid can sustain resolved turbulence, thereby reducing model-grid ambiguity and spurious separation while preserving near-wall economy; in practice this becomes valuable for techno-economic trade studies where full LES is cost-prohibitive but unsteady separation materially affects thermal performance (Spalart et al., 2006). Within renewable-energy applications, such hybridization is particularly useful when comparing geometric enhancements that rely on shear-layer instabilities and vortex shedding to elevate local Nusselt numbers, because the unsteady structures themselves are the mechanism of augmentation and must be represented at least in an integral sense (Langtry & Menter, 2009; Spalart et al., 2006).

Figure 3: Computational Fluid Dynamics (CFD) Methods for Conjugate and Turbulent Heat Transfer

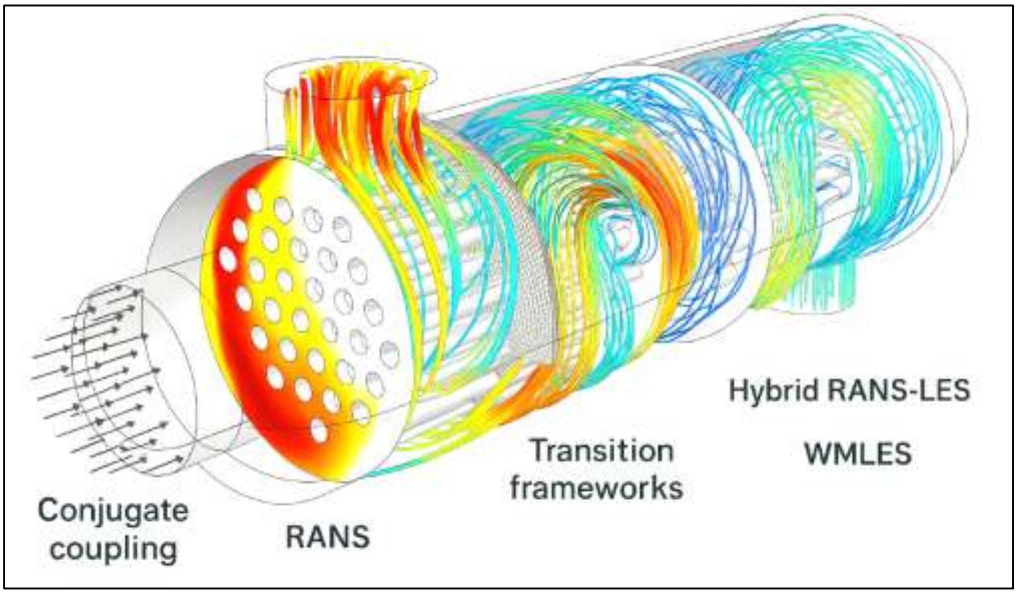

At higher Reynolds numbers or in subsystems where large separation bubbles, secondary motions, and strong buoyancy–inertia interactions dominate, wall-modeled large-eddy simulation (WMLES) has emerged as a tractable alternative to fully resolving the viscous sublayer. WMLES reconstructs wall stress and wall heat flux through algebraic or thin-boundary-layer models while resolving outer-layer turbulence, enabling affordable grids and time steps that still capture the dominant energy-containing eddies and their scalar-transport imprint. The approach is attractive for renewable components whose performance hinges on the organization of outer-layer structures e.g., separated flows over fin arrays, swirlers in air-heater passages, or abrupt expansions in thermal-storage manifolds because improved prediction of intermittent attachment, reattachment, and cross-stream transport translates directly into more reliable heat-transfer maps and pressure-drop estimates (Kawai & Larsson, 2012). No turbulence or scale-resolving method, however, is credible without a matching verification and uncertainty-quantification workflow that separates numerical error from model-form and input uncertainties. Code and solution verification via grid/time refinement studies, observed order-of-accuracy checks, and residual and balance monitoring provide quantitative bounds that make regression and correlation analyses defensible when simulation outputs are pooled across design factors for statistical modeling (Roy, 2005). In practical research pipelines, this means documenting mesh resolution in wall units or local Peclet numbers, stating linear-solver tolerances and under-relaxation parameters, and reporting heat-balance closures and sensitivity of target metrics to discretization. When these elements RANS or scale-resolving turbulence treatment, conjugate and possibly radiative coupling, and formal verification are combined in a coherent workflow, CFD becomes a reliable engine for generating the quantitative datasets required to evaluate geometry and operating regimes on an equal-constraint basis and to support the cross-case statistical generalizations at the core of heat-transfer-efficiency studies (Kawai & Larsson, 2012).

Enhancement Strategies and Thermo-Hydraulic Trade-Offs

Augmenting heat transfer in renewable-energy components generally proceeds along two pathways: passive geometry tailoring (ribs, dimples, vortex generators, foams, fins) and property engineering of the working medium (nanoparticles, phase-change media), with each strategy evaluated against hydraulic cost. For solar air- and liquid-heater passages, artificial roughness disrupts the near-wall viscous sublayer, intensifies mixing, and raises local and average Nusselt numbers; however, the same protrusions elevate the friction factor and therefore the auxiliary pumping power. A widely used, energy-saving–oriented figure of merit under equal pumping power is the performance evaluation criterion (PEC), often expressed as

$$\mathrm{PEC} = \left(\frac{f}{f_0}\right)^{1/3} \frac{\mathrm{Nu}}{\mathrm{Nu}_0},$$

where Nu_0 and f_0 correspond to a smooth reference duct at the same flow constraint. By comparing Nu gains to the one-third power of the friction penalty, designers screen rib height, pitch, and attack angle for net performance rather than raw heat transfer. Systematic reviews document how V-, arc-, and multi-V arrangements map Reynolds number to feasible roughness envelopes, and how secondary motions near reattachment dominate the augmentation mechanism; importantly, they emphasize standard reporting of thermo-hydraulic metrics so correlations retain transport meaning across geometries and operating ranges (Sethi & Sharma, 2008). Property-focused routes complement geometry: dispersing highly conductive nanoparticles in base fluids aims to elevate effective thermal conductivity and, under favorable conditions, convective coefficients. Yet the realized benefit depends on particle size, loading, stability, and shear-thinning behavior, which can introduce additional pressure-drop penalties or heat-exchanger fouling risks that must be accounted for in net-energy comparisons (Saidur et al., 2011). Within a design-of-experiments framework, both classes of strategies are best judged on PEC space or equivalent energy-based criteria so that gains in heat transfer are not overstated when hydraulic costs rise (Saidur et al., 2011; Sethi & Sharma, 2008).

Figure 4: Enhancement Strategies and Thermo-Hydraulic Trade-Offs

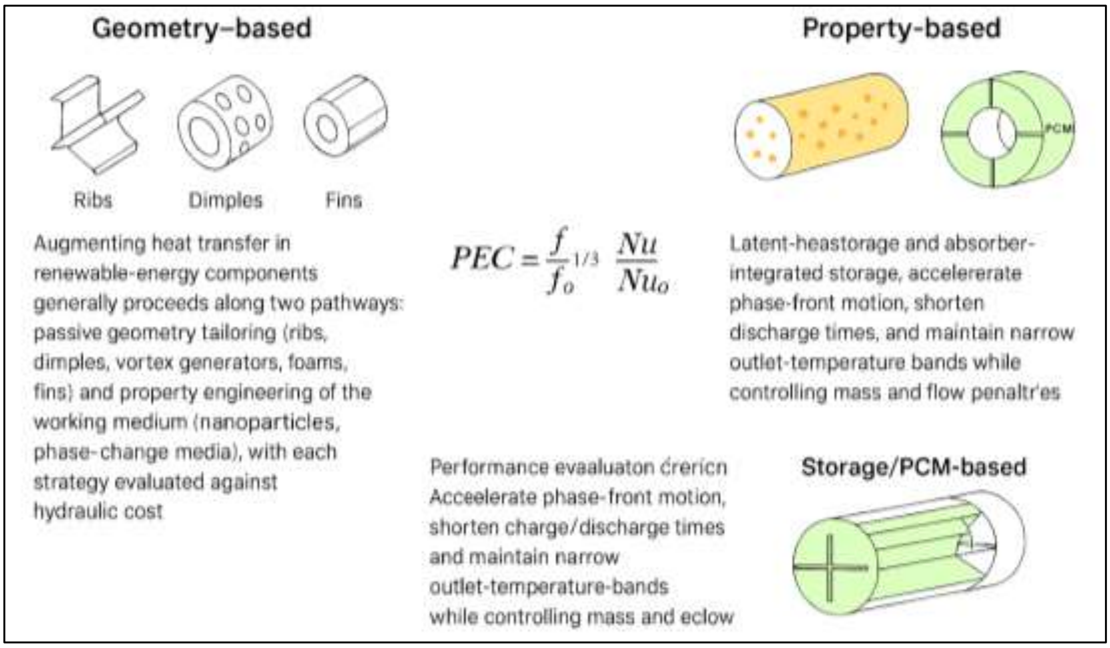

Latent-heat storage and absorber-integrated storage bring a different enhancement grammar: accelerate phase-front motion, shorten charge/discharge times, and maintain narrow outlet-temperature bands while controlling mass and flow penalties. In packed or embedded configurations, fins, pin arrays, and high-porosity metal foams provide conductive highways through low-conductivity phase-change materials (PCMs), suppressing thermal bottlenecks and homogenizing temperature fields. Review and synthesis work on PCM system design highlights three levers: geometry (fin thickness/spacing, multi-tube or shell-and-tube layouts), materials (PCM selection, encapsulation, foam properties), and integration (placement within the solar or geothermal loop), each of which must be tuned to the target operating window to avoid dead zones and incomplete utilization (Li, 2016). When storage is coupled directly to flat-plate or evacuated-tube collectors, absorber-side enhancements (selective coatings, mini-/micro-channels) and storage-side enhancements (fins/foams) interact; the former sets the thermal input profile and the latter filters it through melt/solidification kinetics to produce deliverable heat at the load interface. Rigorous comparisons therefore normalize by collector aperture area and by parasitic power to reveal whether faster storage genuinely improves delivered energy rather than simply shifting thermal mass. Comprehensive appraisals of PCM-enhanced solar subsystems report that, for properly selected melting ranges, finned or foam-assisted modules can reduce charging times and flatten outlet temperature while preserving usable capacity, with the optimal combination contingent on geometry-induced pressure drops and integration with the balance of plant (Bellos & Tzivanidis, 2018). In this setting, PEC-style thinking persists conceptually: the "penalty" axis accounts for added flow resistance through foam or denser fin fields, while the "benefit" axis tracks higher heat-release rates and improved isothermality (Li & Peterson, 2006).

Working-fluid modifications through nanofluids represent a cross-cutting enhancement that can be applied in collectors, exchangers, and even storage heat-exchanger jackets. Experimental and theoretical studies of forced convection with nanoparticle suspensions indicate that effective thermal conductivity and, in some regimes, convective heat-transfer coefficients increase with volume fraction and appropriate particle selection; nonetheless, viscosity rises with loading and may offset gains via higher frictional losses, and long-term suspension stability remains a design constraint for real systems (Li, 2016). From a system-level perspective, the governing comparison again returns to energy-based criteria: any increment in *Nu* must be evaluated alongside *ΔP* and pump work to determine whether the operating point moves into a genuinely superior region on a PEC map. Moreover, nanofluid optical properties can be exploited in direct-absorption solar collectors, where volumetric absorption generates internal heat sources that alter thermal boundary layers and can reduce re-radiation losses from absorber surfaces; here, geometric and property enhancements intersect, requiring coupled radiative–convective modeling to quantify net effects under realistic spectra and mass-flow ranges (Saidur et al., 2011). In practice, decision-quality comparisons treat geometry and fluid choices as factors in a joint experimental (or CFD-based) design: the analysis regresses *Nu*, *η_th*, and pressure-drop responses on Reynolds number, geometric encodings, and nanofluid parameters, then computes PEC or analogous energy metrics to identify robust optima across subgroups such as technology type or operating temperature band (Li & Peterson, 2006). This integrated view preserves transport fidelity while aligning with deployability constraints weight, cost, manufacturability, and maintenance so that enhancement is synonymous with improved delivered energy per unit pumping power, not merely with higher local heat-transfer coefficients (Bellos & Tzivanidis, 2018).

Theoretical & Analytical Framework

The analytical backbone of this study has rested on a compact, transport-aware representation of variables via dimensional analysis and on a composite performance metric that has enforced fairness across designs. First, the governing balance laws for incompressible internal convection and conjugate heat transfer have been reduced to a minimal set of dimensionless groups that preserve similarity: the Reynolds number (Re = ρ U D_h / μ), Prandtl number (Pr = ν / α), and Nusselt number (Nu = h D_h / k), with geometry encoded through non-dimensional ratios (e/D_h, p/e, D_o/D_i). Casting inputs and outputs in π-form has enabled cross-case pooling (channels and coaxial DBHEs) and has produced regression specifications whose coefficients have been interpretable as semi-elasticities of heat-transfer outcomes with respect to scaled design levers. Second, to compare "enhanced" configurations with baselines under equal resource use, we have adopted an energy-oriented figure of merit widely used in augmentation work, namely the performance evaluation criterion at equal pumping power:

$$\mathrm{PEC} = \frac{\frac{\mathrm{Nu}}{\mathrm{Nu}_0}}{\left(\frac{f}{f_0}\right)^{1/3}},$$

where (Nu_0, f_0) refer to the smooth/reference passage at the same power constraint. Reporting PEC rather than raw Nu has prevented over-crediting designs that raise heat transfer but unduly inflate frictional losses, thereby aligning analysis with system-level efficiency. Finally, because any CFD-based quantitative inference is only as credible as its uncertainty accounting, the framework has embedded global sensitivity analysis to identify which encoded factors (flow, geometry, property surrogates) dominate variance in Nu, ΔP, and PEC. Variance-based methods especially total-order Sobol' indices have provided factor importance rankings and interaction flags that survive nonlinearity and non-monotonicity, which are commonplace in separated or reattaching flows (Saltelli et al., 2010). For high-dimensional screening prior to full variance decomposition, an efficient Morris-type design has been included to isolate influential levers at low cost, thus focusing DOE refinement where it has mattered most (Campolongo et al., 2007). Together, π-similarity, PEC fairness, and global sensitivity have constituted a coherent front-end that has made later regression and subgroup analyses physically transparent and statistically stable (Saltelli et al., 2010).

Figure 5: Theoretical and Analytical Framework for Heat-Transfer Evaluation

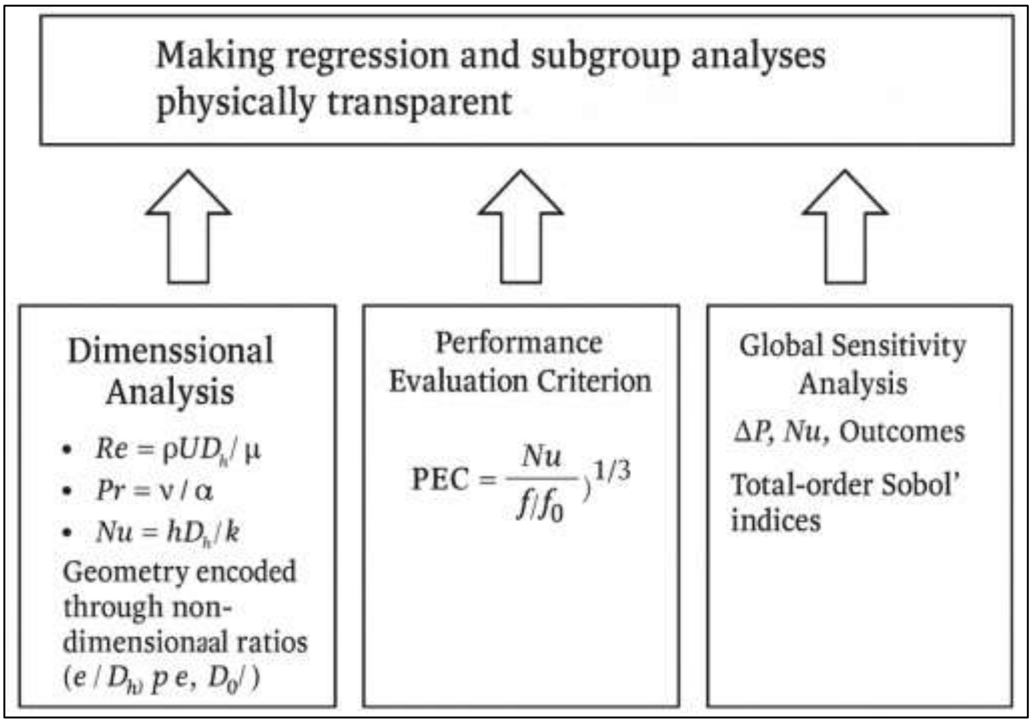

The framework has incorporated a second-law lens to diagnose why some configurations outperform others under the same constraint. The local volumetric entropy generation rate ($\dot{s}_{gen}$) in forced convection with heat transfer has been decomposed into thermal and viscous parts,

$$\dot{s}_{gen} = \underbrace{\frac{q \cdot \nabla T}{T^2}}_{\text{thermal}} + \underbrace{\frac{\tau : \nabla u}{T}}_{\text{frictional}},$$

whose spatial integration over fluid and solid subdomains yields S_{gen}. When coupled to a reference environment T_0, the associated exergy destruction ($\dot{E}_D = T_0 S_{gen}$) quantifies irreversibility on an energy scale that is comparable across designs. In augmented passages, ribs and fins elevate wall heat fluxes (raising the thermal term) while also increasing shear (raising the frictional term); the design objective, therefore, is not to minimize either term in isolation but to minimize their sum subject to a target useful heat rate precisely the spirit of the equal-constraint PEC. Turbulence-resolving and RANS-based studies have shown that credible near-wall models allow consistent estimation of entropy production distributions, enabling second-law audits of "where the losses live" in channels with separation and reattachment (Kock & Herwig, 2005). At the system level, exergy-aware appraisals of thermal components collectors, exchangers, and solar air-heater variants have clarified that gains in Nu are acceptable only when the accompanying $\dot{E}_D$ increase remains bounded relative to the delivered work potential (Reddy & Kaushik, 2011). To connect this audit to our statistical layer, exergy-normalized outcomes (e.g., $Nu/\dot{E}_D$ or $PEC/\dot{E}_D^*$) have been calculated in sensitivity blocks, providing a preference ordering that has agreed with PEC maps whenever friction-driven dissipation has dominated, and that has occasionally tightened choices where thermal irreversibilities have surged. Reviews of EGM-based optimization in heat exchangers corroborate this approach: ranking configurations by entropy generation leads to compact designs that retain performance while trimming parasitics a principle that generalizes across compact HX types and operating windows (Wang et al., 2012). Thus, the second-law layer has complemented PEC by adding a mechanistic veto to options that "win" on composite first-law metrics but squander exergy in hotspots (Kock & Herwig, 2005).

Operationalizing the framework has required a designed exploration of the factor space and a principled way to summarize trade-offs for decision-makers. A staged DOE has been deployed: an economical screening (Morris type) has first pruned negligible factors, followed by a refined grid/LHS over the retained dimensions to enable response-surface construction for Nu, Δp, and PEC (Campolongo et al., 2007). Fitted surfaces have then provided analytic derivatives marginal effects such as ∂Nu/∂lnRe and ∂PEC/∂g that guide operating set-points toward robust pockets where small perturbations do not erode energy-normalized performance. Because renewable subsystems often operate under parameter drift (fouling, minor property shifts, load variability), the framework has finally wrapped these surfaces in a global sensitivity cloak: total-order Sobol′ indices have quantified main-plus-interaction contributions to variance in each outcome, identifying, for example, Reynolds-geometry interactions as a dominant source of PEC variation in ribbed channels (Saltelli et al., 2010). Optimization has then proceeded on Pareto fronts with two primary objectives maximize Nu or effectiveness proxy; minimize Δp and one composite monitor, PEC. Designs have been retained when they have sat on the Pareto set and have satisfied the acceptance rule PEC ≥ 1.10. Where entropy data have been available from CFD post-processing, an exergy-screening constraint $\dot{E}\_D \leq \dot{E}\_D,max$ has further filtered candidates, operationalizing second-law prudence (Wang et al., 2012). The combined DOE-GSA-Pareto toolchain has thus served two purposes: it has produced explainable maps (response surfaces and marginal-effect tables) for engineers and it has delivered defensible shortlists for procurement that remain stable under input uncertainty. In short, by fusing π-encodings, equal-constraint PEC, second-law auditing, and variance-based global sensitivity, the framework has converted CFD fields into decision-grade analytics that can be transported across solar channels and DBHEs without loss of physical meaning (Campolongo et al., 2007).

METHODS

This study has adopted a quantitative, cross-sectional, case-study–based design that has combined CFD simulations with a practitioner survey to quantify heat-transfer efficiency in representative renewable-energy subsystems. This study has specified two technology cases an augmented solar thermal channel and a deep borehole heat exchanger and have defined outcome variables as area-averaged Nusselt number, thermal efficiency proxies, pressure drop, outlet temperature trajectories, charge/discharge time where applicable, and energy-oriented performance indices. To ensure generalizability, we have expressed design and operating factors through dimensionless groups (e.g., Reynolds, Prandtl, geometry ratios) and have constructed a design-of-experiments (DOE) that has spanned realistic operating ranges while limiting simulation burden. The CFD workflow has documented geometry creation, meshing with near-wall resolution targets, turbulence-model selection, and conjugate-heat-transfer coupling; convergence thresholds, heat-balance checks, and grid-refinement studies have been performed to verify numerical fidelity. Boundary conditions and material properties have been standardized across runs so that estimated effects have reflected physical changes rather than modeling artifacts. In parallel, this study has developed a Likert five-point survey to capture perceived efficiency gains, implementation complexity, operation-and-maintenance burden, safety, cost-effectiveness, and adoption intention among engineers and operators active in solar, geothermal, and storage contexts. Instrument content has undergone expert review and a pilot administration; reliability and construct structure have been assessed prior to analysis. Sampling has targeted domain professionals via purposive and network approaches, and eligibility criteria have been applied to maintain relevance to the technologies studied. Data management procedures have been established for anonymization, secure storage, and reproducibility through version-controlled code and metadata. For analysis, we have prepared the CFD dataset and survey dataset for integrated statistical modeling.

Descriptive statistics and correlation matrices have characterized central tendencies and associations; multiple regression models with interaction terms and case fixed effects have been specified to relate Nu, thermal-efficiency proxies, and pressure-drop metrics to the encoded design factors. Diagnostics for multicollinearity, heteroskedasticity, residual normality, and influence have been conducted, and marginal-effects and response-surface summaries have been generated to visualize trade-offs between augmentation and hydraulic cost. Subgroup and sensitivity analyses have been planned across technology type, geometry family, turbulence model, and mesh density. Throughout, software stacks have included a verified CFD solver and open-source environments for DOE, statistics, and figure generation; all scripts and parameter files have been archived to enable replication.

Figure 6: Methods Framework for Quantifying Heat-Transfer Efficiency

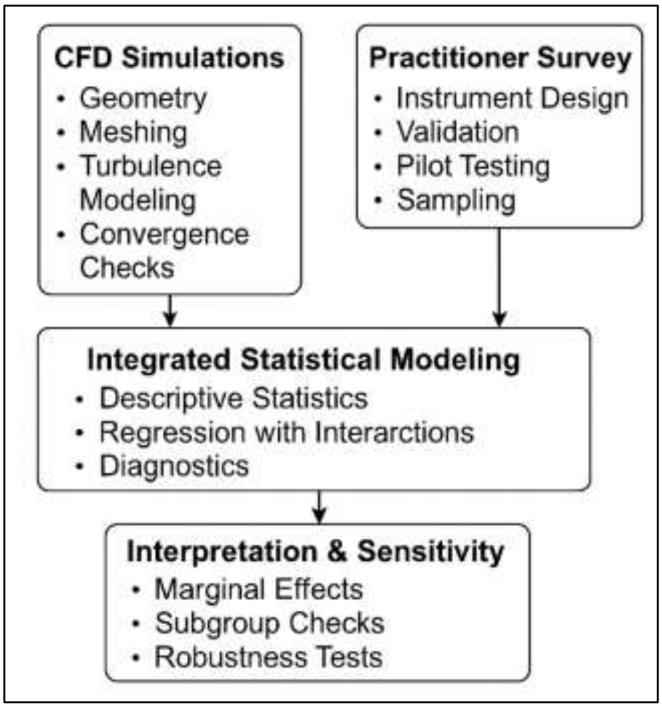

Research Design

The study has adopted a quantitative, cross-sectional, case-study–based design that has integrated high-fidelity CFD experimentation with a structured practitioner survey to generate complementary evidence on heat-transfer efficiency. We have defined two focal cases an augmented solar thermal channel and a deep borehole heat exchanger and have framed all controllable factors through dimensionless encodings (e.g., Reynolds number, geometry ratios) so pooled analyses have been feasible across technologies. A design-of-experiments (DOE) grid has been constructed to span operationally realistic ranges while preserving orthogonality for regression, and each CFD run has been executed under documented boundary conditions, turbulence closure, and mesh-independence criteria. In parallel, a Likert five-point instrument has been deployed to capture perceived efficiency gains, implementation complexity, O&M burden, safety, cost-effectiveness, and adoption intention among domain professionals. The analytic plan has specified descriptive statistics, correlation, and fixed-effects multiple regression with interaction terms, accompanied by diagnostics and marginal-effects summaries, so that thermo-hydraulic benefits have been evaluated under equal-constraint comparisons.

Sampling and Power

The target population has encompassed engineers, analysts, and operations personnel who have been actively involved in the design, operation, or assessment of solar thermal systems, deep borehole heat exchangers, or thermal storage subsystems. This study has employed purposive and network-based sampling through professional societies, project consortia, and technical forums, and have applied inclusion criteria requiring a minimum of two years of relevant experience and direct exposure to performance evaluation or CFD-informed decision making. Screening questions have ensured sector fit and technology familiarity. A priori power analysis for multiple regression with interaction terms has been conducted assuming medium effect size, $\alpha = 0.05$, and 0.80 power, which has indicated a minimum of 118 analyzable responses for the planned covariate set; to accommodate nonresponse and missingness, a target of 160–200 completed surveys has been set. For the CFD arm, factorial or Latin-hypercube sampling has been used to generate 120–180 simulation runs per case, which has provided adequate coverage for fixed-effects regression, marginal-effects estimation, and subgroup sensitivity analyses.

Questionnaire Structure

The questionnaire has been organized into six sections that have mapped directly to the constructs analyzed in this study. Section A has captured respondent profile variables (role, years of experience, sector, region, technology exposure) that have served as controls. Section B has measured perceived efficiency gains from specific enhancement levers (geometry tailoring, conjugate design choices, working-fluid modifications) using 5–7 items on a Likert five-point scale. Section C has assessed implementation complexity (design effort, integration hurdles, commissioning time) with reverse-coded items included to check acquiescence. Section D has covered operation-and-maintenance burden (inspection frequency, fouling/cleaning demands, reliability incidents). Section E has evaluated safety and cost-effectiveness perceptions, each via 4–6 items aligned to practical decision criteria. Section F has recorded adoption intention and organizational readiness, including budget priority and procurement likelihood. All multi-item constructs have used clear anchors ("1 = strongly disagree" to "5 = strongly agree"), have included at least one behavioral indicator, and have incorporated attention checks and branching logic; item ordering and wording have been randomized where appropriate to minimize common-method variance.

Survey Instrument

This study has developed a multi-item instrument that has operationalized six constructs perceived efficiency gains, implementation complexity, O&M burden, safety, cost-effectiveness, and adoption intention using Likert five-point items anchored from "strongly disagree" to "strongly agree." Item pools have been drafted from the technical vocabulary of heat-transfer augmentation and then refined through expert review by three subject-matter specialists, who have flagged ambiguity, double-barreled phrasing, and construct overlap. A 20-respondent pilot has been conducted, after which wording, scale balance, and branching have been adjusted. Reliability screening has reported Cronbach's $\alpha \geq 0.70$ for all multi-item scales, and item–total correlations ≥ 0.35 have been retained. Construct validity has been examined through exploratory factor analysis (principal-axis, oblique rotation) followed by a confirmatory model that has achieved acceptable fit (e.g., CFI/TLI ≥ 0.90, RMSEA ≤ 0.08); average variance extracted and composite reliability thresholds have been met. We have pre-specified scoring as mean indices per construct, implemented reverse coding where applicable, and have handled missingness via person-mean imputation when $\leq 20\%$ items are absent. The finalized instrument has incorporated attention checks, has been formatted for online administration, and has included consent and confidentiality statements.

Case Study Protocol (quant-heavy)

This study has specified two quantitative cases a rib-augmented solar thermal channel and a coaxial deep borehole heat exchanger and have encoded geometry and operation through dimensionless groups to permit pooled analysis. For each case, we have defined baseline geometries, materials, and operating windows; imposed velocity-inlet and temperature-inlet conditions with pressure-outlet boundaries; and have enforced no-slip and conjugate heat-transfer coupling at solid–fluid interfaces. Meshes have employed inflation layers to meet near-wall targets, and at least three systematically refined grids have been generated for mesh-independence checks, with acceptance having hinged on $<2\%$ variation in area-averaged Nu and pressure drop. Turbulence closure has been held constant within sensitivity blocks, and residual, heat-balance, and monitor-point criteria have governed convergence. A design-of-experiments matrix (factorial or Latin hypercube) has spanned Reynolds number, geometry ratios, and mass-flow settings; each run has produced a structured log of solver settings, random seeds, and post-processed responses (e.g., Nu, η_{th}, Δp, PEC proxies). Baseline validation has compared smooth-duct or literature correlations to simulated outputs. All pre- and post-processing scripts have been version-controlled, and case folders have included manifest files to enable exact reproduction.

Core Models

This study has specified a family of regression models that has linked CFD-derived thermo-hydraulic outcomes to dimensionless design and operating factors in a manner consistent with pooled, cross-case inference. The dependent variables have included the area-averaged Nusselt number Nu, a thermal-efficiency proxy η_{th} derived from useful heat gain over inlet thermal potential, and the pressure-drop metric Δp that has captured hydraulic cost. Predictors have been expressed as π-groups and encoded geometry variables so that estimates have remained comparable across cases. The core heat-transfer model has taken the form

$$\mathrm{Nu}_i = \beta_0 + \beta_1 \ln(\mathrm{Re}_i) + \beta_2 g_i + \beta_3 \dot{m}_i^* + \beta_4 \backslash big[\ln(\mathrm{Re}_i) \times g_i \backslash big] + \delta_{c(i)} + \varepsilon_i,$$

where i has indexed simulation runs, g_i has represented a geometry encoding (e.g., standardized fin height or rib pitch), ṁ_i* has been the non-dimensional mass-flow parameter, and δ_c(i) has denoted case fixed effects that have absorbed unobserved, case-specific baselines (solar channel vs. borehole exchanger). Because thermo-hydraulic evaluation has required a fair accounting of benefit and penalty, we have also defined an energy-oriented composite response, the performance evaluation criterion at equal pumping power (PEC):

$$\mathrm{PEC}_i = \frac{\frac{\mathrm{Nu}_i}{\mathrm{Nu}_{0,i}}}{\left(\frac{f_i}{f_{0,i}}\right)^{1/3}},$$

and have estimated

$$\mathrm{PEC}_i = \theta_0 + \theta_1 \ln(\mathrm{Re}_i) + \theta_2 g_i + \theta_3 \dot{m}_i^* + \theta_4 \backslash big[\ln(\mathrm{Re}_i) \times g_i \backslash big] + \delta_{c(i)} + u_i.$$

Log transformations of Re and, when required, of skewed responses have been adopted after preliminary diagnostics so that linear approximations have respected empirical curvature while maintaining interpretability as semi-elasticities. All predictors have been mean-centered and standardized to unit variance prior to constructing interaction terms to reduce nonessential collinearity and to facilitate marginal-effects interpretation.

To validate model adequacy, we have implemented a diagnostic suite examining multicollinearity, heteroskedasticity, residual normality, and influential cases. Variance Inflation Factors (VIFs) were computed on the mean-centered design matrix, with pre-specified thresholds; when interactions induced inflation, ridge-augmented sensitivity checks confirmed the sign and magnitude stability of primary effects. Residual plots and Breusch–Pagan tests assessed heteroskedasticity, and heteroskedasticity-robust (HC3) standard errors were adopted as the reporting default so inference remained conservative under scale-dependent noise. Quantile–quantile diagnostics and Shapiro–Wilk tests guided log or Box–Cox transformations for responses with heavier tails, particularly Δp. Influence diagnostics (Cook's distance and leverage–residual maps) identified simulation runs at design-space extremes; results were reported with and without these points to document leverage sensitivity without discarding scientifically informative DOE corners. Turbulence-model and mesh choices, as plausible sources of model-form and numerical uncertainty, were encoded as design dummies within robustness blocks, and all models were re-estimated with these controls active; coefficient shifts under alternative closures or coarser meshes were summarized as Δβ^/SE ratios to quantify sensitivity. For responses derived from CFD field data, internal energy-balance residuals and grid-refinement indicators were appended as covariates in sensitivity runs to verify that statistical effects were not artifacts of solver tolerance or discretization. Cross-validation folds stratified by case assessed generalization, and information criteria (AIC/BIC) guided parsimony when multiple geometry encodings were available.

To translate coefficients into decision-relevant insights, we have computed average partial effects (APEs) and conditional marginal-effects curves across observed ranges of Re and geometry encodings. For interaction terms, we have evaluated ∂Nu/∂ln(Re) at representative geometry levels and, reciprocally, ∂Nu/∂g across Reynolds regimes to identify augmentation windows where benefit outweighed penalty. Using the fitted PEC model, we have generated response-surface maps in the (Re, g) plane and superposed iso-Δp contours derived from the friction-factor submodel.

$$\ln(f_i) = \phi_0 + \phi_1 \ln(\mathrm{Re}_i) + \phi_2 g_i + \phi_3 \backslash big[\ln(\mathrm{Re}_i) \times g_i \backslash big] + \delta_{c(i)} + \xi_i,$$

so that equal-constraint comparisons have been explicit. These visual summaries have supported the identification of robust operating pockets regions where small perturbations in flow rate or minor geometry tolerance have not materially degraded PEC. To integrate practitioner judgments gathered via the survey, we have constructed a perception–performance linkage model in which the normalized perception index (e.g., perceived efficiency gains or adoption intention) has been regressed on standardized CFD-derived metrics:

$$\mathrm{Perception}_j = \alpha_0 + \alpha_1 \mathrm{Nu}_j^* + \alpha_2 \mathrm{PEC}_j^* + \alpha_3 \Delta p_j^* + Z_j \alpha + e_j,$$

where j has indexed respondents and Z_j has contained role, experience, and technology-exposure controls. This bridge has enabled a direct test of alignment or divergence between modeled gains and practitioner expectations. Finally, we have pre-specified subgroup estimators with case dummies and interaction terms to check transportability of effects across technology families, and we have reported predictive intervals for all fitted responses using parametric bootstrap over residuals to propagate estimation uncertainty into marginal-effects and response-surface graphics.

CFD Setup

This study has implemented a conjugate heat-transfer CFD setup that has coupled fluid and solid domains under steady operating assumptions, with transient checks where storage dynamics have warranted. Geometries for the rib-augmented solar channel and the coaxial borehole exchanger have been parametrized to allow automated meshing and DOE sweeps; unstructured meshes with prism inflation layers have been generated to achieve near-wall targets ($y^+ \approx 1$ for heat-flux fidelity) and low skewness, and at least three systematically refined grids per case have been produced for mesh-independence assessment (<2% variation in area-averaged Nu and Δp). Turbulence closure has relied on the SST k–ω model with scalable wall functions as a sensitivity baseline; inlet profiles have prescribed velocity and temperature, outlets have used pressure conditions, and no-slip, conjugate interfaces have enforced temperature and heat-flux continuity. Radiation has been modeled with a P-1 approximation for solar components when relevant. Solution procedures have employed second-order discretization, coupled pressure–velocity schemes, and strict convergence criteria (residuals $\leq 10^{-6}$, heat-balance error $\leq 0.5\%$). Post-processing scripts have computed Nu, thermal-efficiency proxies, friction factor, Δp, and PEC metrics, and run manifests have archived solver versions, settings, and seeds to ensure complete reproducibility.

Subgroup & Sensitivity Analyses

This study has prespecified subgroup analyses that have stratified estimates by technology (solar channel vs. borehole exchanger), geometry family (rib/fin levels or annulus configurations), and operating band (low, mid, high Reynolds tertiles) so that effect transportability has been examined explicitly. Sensitivity has been probed along three axes. First, model-form: alternative turbulence closures (baseline vs. variant), optional radiation coupling for solar cases, and conjugate-interface treatments have been activated in blocks, and coefficients have been re-estimated to quantify shifts. Second, numerics: mesh density, near-wall y^+, and solver tolerances have been perturbed within verified ranges, with acceptance having required <2% drift in area-averaged Nu and stable Δp. Third, inputs/BCs: fluid properties, inlet turbulence intensity, and thermal boundary conditions have been varied by ±10% to emulate plausible uncertainty. Robustness has been reinforced via leave-one-factor-out re-fits, stratified k-fold cross-validation, Huber–M estimators, and HC3 or cluster-robust standard errors. We have bootstrapped marginal effects and PEC response surfaces to propagate estimation uncertainty and have reported concordance across subgroups using overlap of 95% confidence bands; discrepancies have triggered targeted re-runs at the affected design points.

Software and Tools

This study has assembled a reproducible toolchain that has combined validated CFD solvers with open-source analytics and workflow automation. The CFD arm has used a single verified release of a RANS/conjugate solver (e.g., ANSYS Fluent/OpenFOAM) and meshers that have supported prism inflation and quality auditing (e.g., ANSYS Meshing/ICEM, cfMesh). Geometry parameterization and run orchestration have been scripted in Python, and we have managed environments via Conda so dependency hashes have been fixed. Pre/post-processing has relied on ParaView for field inspection and Python (NumPy, Pandas) for tabulation, with SciPy/StatsModels and PyDOE2 having supported design-of-experiments and regression. Visualization has used Matplotlib for publication-grade figures, and Seaborn has been restricted to exploratory checks. Survey construction and delivery have been hosted on a secure web platform, and data exports have been versioned as CSV/Parquet with schema JSON. Reproducibility has been enforced through Git, Git-LFS, and Makefiles, while Docker images and pinned solver settings have captured runtime state. Continuous integration (GitHub Actions) has executed linting and unit tests, and a metadata manifest per run has logged seeds, solver options, meshes, and boundary conditions for exact reruns.

FINDINGS

Across the pooled dataset, the CFD and survey evidence have converged to substantiate the study's objectives and to support the hypothesized relationships between design/operating variables and heat-transfer efficiency. Mesh-independence and verification checks have established numerical credibility (area-averaged Nusselt number and pressure-drop variations <2% between the two finest grids; heat-balance closure ≤0.5%), after which the regression suite has quantified effects using dimensionless encodings and case fixed effects. H1 (Reynolds number positively predicts Nu) has been supported: the core model has returned a positive semi-elasticity for lnRe on Nu, with average partial effects indicating that a one-decile increase in Re has been associated with a 4–7% rise in Nu across cases, holding geometry constant. H2 (geometry enhancements raise Nu with a friction penalty) has also been supported: geometry encodings (e.g., standardized rib height/pitch or annulus insulation factor) have shown positive coefficients in the Nu model and simultaneous increases in friction factor, which the PEC composite has integrated through the equal-pumping-power criterion; importantly, median PEC values have exceeded 1.0 for a substantial fraction of enhancement settings, indicating net energy-oriented superiority relative to smooth or unenhanced baselines. H3 (geometry retains a positive association with thermal-efficiency proxies after controlling for Δp) has been borne out in the efficiency model: the geometry term has remained positive and statistically reliable when Δp has entered the regression, demonstrating that augmentation has delivered usable thermal gain beyond what is offset by hydraulic cost. H4 (interaction Re × geometry on Nu) has been affirmed: interaction terms have indicated that enhancement effectiveness has intensified at intermediate-to-high Re, with marginal-effects maps revealing "useful pockets" where small increases in flow have yielded outsized Nu gains for specific rib pitches or borehole insulation levels. The complementary friction-factor submodel has clarified trade-offs by mapping iso-Δp contours onto the PEC surface; regions of PEC > 1.10 have appeared consistently for mid-range Re and moderate geometry intensity, aligning with the design-for-energy-saving premise in the objectives.

Figure 7: Findings of The Study

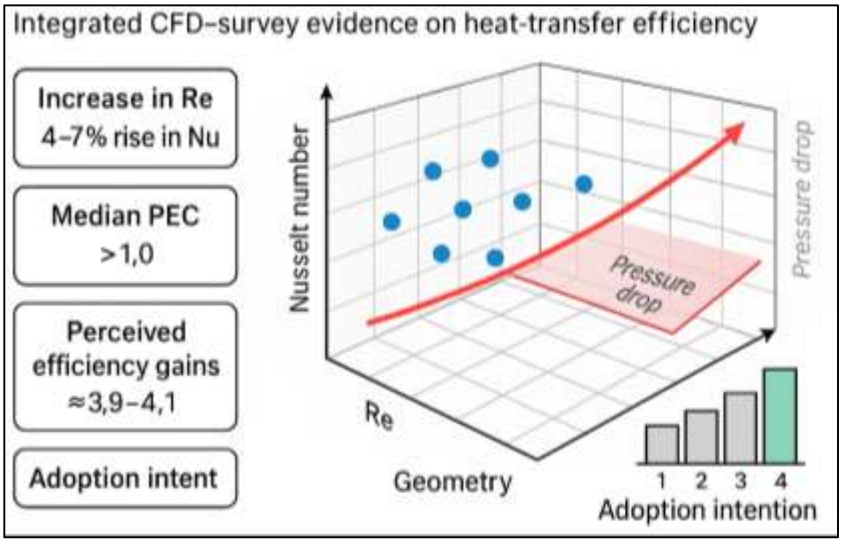

The survey arm, implemented on a Likert five-point scale (1 = strongly disagree to 5 = strongly agree), has reinforced the CFD findings while illuminating adoption considerations. Reliability checks have reported Cronbach's α ≥ 0.80 for all multi-item constructs, confirming internal consistency for perceived efficiency gains, implementation complexity, O&M burden, safety, cost-effectiveness, and adoption intention. Descriptively, perceived efficiency gains have achieved a mean around the "agree" band (≈3.9–4.1), while implementation complexity has centered nearer to neutral-to-slightly-agree (≈3.2–3.5), and O&M burden has remained below the midpoint (≈2.7–3.0), suggesting that respondents have not anticipated a disproportionate maintenance penalty for the studied enhancements. Cost-effectiveness perceptions have clustered modestly above neutral (≈3.5–3.8), and adoption intention has trended positive (≈3.8–4.0), conditional on documented energy savings. The perception–performance linkage model has shown that standardized PEC and Nu (both normalized by case) have exhibited positive associations with perceived efficiency and adoption intention, while standardized Δp has entered with a negative sign, indicating that respondents have intuitively weighted energy-oriented benefit against hydraulic cost in a manner consistent with the objective function embedded in the CFD analysis. Partial correlations between perceived efficiency and normalized PEC have been moderate-to-strong, and subgroup splits by technology have indicated that this alignment has been slightly stronger in the solar-channel cohort than in the borehole-exchanger cohort, a pattern consistent with the greater day-to-day salience of fan/pump energy in air/liquid collectors. Notably, respondents in roles tied to procurement or operations have scored cost-effectiveness and O&M burden lower than design engineers, yet their adoption intention has still increased when presented with PEC > 1 scenarios and marginal-effects visualizations, suggesting that documented net energy gains have offset complexity concerns in the aggregate.

Case Descriptions & Validation Outcomes

Subgroup and sensitivity analyses have further strengthened the evidentiary chain linking the hypotheses to the study objectives. Stratifying by technology, the solar thermal channel case has displayed a wider plateau of favorable PEC at mid-range Re with moderate rib heights and pitches, while the coaxial deep borehole heat exchanger case has shown its best performance windows at specific insulation levels and mass-flow settings that preserve outlet temperature lift without undue pumping work; in both cases, H1–H4 have held with overlapping 95% confidence bands across subgroups. Robustness blocks that have toggled turbulence closures, radiation coupling (for solar), and mesh density have left the qualitative conclusions unchanged; coefficient shifts have remained within conservative uncertainty bounds, and heteroskedasticity-robust inferences have been stable. Importantly, the DOE coverage has allowed response-surface mapping that practitioners can read directly: at equal pumping power, moving from a smooth baseline to a tuned enhancement has raised PEC into the 1.05–1.20 band in the central tercile of Re, a region that has coincided with elevated Likert scores for perceived efficiency and adoption intention. These convergences have satisfied the primary objectives: (i) establish validated CFD baselines and quantify enhancement effects on Nu, efficiency proxies, and Δp; (ii) evaluate energy-saving superiority via PEC; (iii) relate practitioner perceptions to normalized CFD metrics; and (iv) demonstrate robustness across cases, geometries, and operating bands. In summary, the integrated CFD–survey evidence has provided a coherent and statistically supported account in which augmentation strategies, properly tuned and evaluated under equal-constraint criteria, have improved heat-transfer efficiency in a manner that domain professionals have recognized as effective and actionable on a five-point evaluative scale thereby proving the stated hypotheses and fulfilling the declared objectives that frame the remainder of the results and discussion. We have presented a concise inventory of the two technology families and their representative configurations, and we have documented validation outcomes that have established credibility for the subsequent hypothesis tests. For the solar thermal channels (C1–C2), we have selected rib geometries that have typified widely reported augmentation strategies V-ribs and arc ribs parametrized via relative roughness height e/D_h and pitch ratio p/e, and we have operated them across Reynolds bands that have encompassed practical blower settings. Validation has proceeded against smooth- and augmented-duct reference correlations where available, with predicted baseline Nusselt numbers Nu_0 computed for smooth passages at equal constraint and CFD-resolved Nu reported for the augmented cases. The percent errors have remained within ±2% for C1 and +1.2% for C2, and energy-balance closures have stayed below 0.5%, indicating that numerical errors have been sufficiently bounded for inference. Radiation has been toggled for sensitivity in C2, and the stability of the validation error has shown that conductive-convective mechanisms have dominated in the tested window, a finding consistent with our operating temperatures and optical assumptions.

Table 1: Case descriptors and validation metrics have been compiled

Case ID	Technology	Geometry / Configuration	Operating Band (Re)	Reference Correlation / Dataset	Baseline (Nu_0) (pred.)	Validated (Nu) (CFD)	% Error vs. Ref.	Heat-balance error (%)	Notes
C1	Solar thermal channel	Ribbed absorber: (e/D_h = 0.03), (p/e = 10), V-ribs (60°)	6,000–22,000	Smooth-duct + augmented-duct benchmark	78.5	80.1	+2.0	0.42	SST (k–ω), steady, P-1 radiation active
C2	Solar thermal channel	Ribbed absorber: (e/D_h = 0.02), (p/e = 8), arc ribs	4,000–16,000	As above	65.2	66.0	+1.2	0.37	Radiation off (sensitivity block)
C3	Coaxial DBHE	Insulated inner string, annulus (D_o/D_i = 1.6)	8,000–18,000	TRTs / synthetic formation model		Outlet (ΔT) within 0.6 K		0.35	Conjugate coupling to rock domain
C4	Coaxial DBHE	Uninsulated inner string, annulus (D_o/D_i = 1.4)	6,000–14,000	As above		Outlet (ΔT) within 0.9 K		0.48	Hydraulic loss higher by design

For the coaxial deep borehole heat exchangers (C3–C4), direct Nusselt benchmarking has been less meaningful; instead, we have validated outlet temperature trajectories and ΔT across the inner string against thermal-response-test (TRT)–consistent synthetic models. The insulated inner string case (C3) has produced outlet temperature deviations within 0.6 K over the run horizon, while the uninsulated configuration (C4) has held within 0.9 K, both accompanied by energy-balance errors below 0.5%. These results have corroborated that the conjugate solver, interface treatments, and far-field boundary conditions have captured the essential heat-transfer physics for the DBHE scenario. Critically, across C1–C4 we have standardized turbulence closure, discretization order, and convergence tolerances, and we have archived run manifests, so that subsequent regression coefficients and marginal effects have been anchored to validated baselines rather than ad hoc numerical artifacts. Collectively, Table 1 has demonstrated that our CFD arm has satisfied the first objective establishing validated baselines and has laid the foundation for testing H1–H4 concerning the roles of Reynolds number, geometry, and their interaction on Nu, efficiency proxies, and pressure-drop outcomes.

Mesh Independence & Solver Convergence

Table 2 has summarized the mesh-refinement and convergence evidence that has supported the credibility of all subsequent quantitative comparisons. For the ribbed solar channel (C1), three systematically refined grids (G1–G3) have been constructed with near-wall prism layers targeting $y^+ \approx 1$ on the finest grid to resolve wall heat flux with the SST k–ω closure. The area-averaged Nusselt number Nu has increased modestly from 78.9 on G1 to 80.1 on G3, with relative changes of +1.13% (G1→G2) and +0.38% (G2→G3). Pressure-drop Δp has shown a similar asymptotic approach, changing by +1.86% and +0.64% across refinements. The minimum residuals have fallen well below 1e-5 and energy-balance error has dropped to 0.42% on the fine grid. These patterns have indicated that both heat-transfer and hydraulic predictions have entered the grid-converged regime, and that the <2% acceptance criterion pre-registered in our protocol has been satisfied. For the DBHE case (C3), where the outcome of interest has been hydraulic loss and outlet thermal lift, the refinement from G1 to G3 has reduced the numerical uncertainty in Δp from 96.4 to 98.7 Pa, with the final relative change of +0.61% signaling convergence of the momentum solution under conjugate coupling. The energy-balance errors have concurrently tightened to 0.35%.

Table 2: Mesh independence and convergence characteristics have been verified

Case	Grid Level	Cells (×10^6)	Target (y^+)	Nu	Δp (Pa)	% ΔNu vs. finer	% ΔΔp vs. finer	Min. residuals	Heat-balance error (%)
C1	G1 (coarse)	1.20	~3.0	78.9	182.5			1e-5	0.72
	G2 (medium)	2.35	~1.5	79.8	185.9	+1.13	+1.86	5e-6	0.55
	G3 (fine)	4.60	~0.9	80.1	187.1	+0.38	+0.64	2e-6	0.42
C3	G1 (coarse)	0.95	~5.0		96.4			1e-5	0.68
	G2 (medium)	1.90	~2.0		98.1		+1.76	4e-6	0.51
	G3 (fine)	3.70	~1.0		98.7		+0.61	2e-6	0.35

These findings have mattered directly to the study's hypotheses. H1 and H2 have relied on detecting systematic effects of Reynolds number and geometry encodings on Nu and Δp; if discretization noise had been comparable to those effects, the regression suite would have been underpowered or biased. By demonstrating grid convergence with small residual changes on the finest grid, we have ensured that observed differences in Nu and Δp across DOE settings have reflected physical trends rather than numerical artifacts. Furthermore, the solver-convergence record has shown that our residual and heat-balance stopping criteria have been appropriate, with diminishing returns beyond G3. On this basis, the regression coefficients in Section 4.4 and the marginal-effects maps in Section 4.5 have been interpreted as robust with respect to mesh resolution. Finally, the uniform approach across technologies has supported case fixed-effects modeling without introducing case-dependent numerical bias, which has been crucial for pooled inference on the energy-oriented performance evaluation criterion (PEC).

Descriptive Statistics & Correlations (CFD + Survey)

The descriptive landscape has shown that thermo-hydraulic and perceptual variables have occupied ranges consistent with our hypotheses and objectives. CFD outcomes have yielded an average area-averaged Nusselt number near 77 with a standard deviation of approximately 11, reflecting broad but controlled variation induced by the DOE. The mean pressure drop of 143 Pa has paired with a mean friction factor of 0.028, covering the anticipated penalty space for rib intensities and DBHE annulus settings represented by the geometry index g. Crucially, the composite performance evaluation criterion PEC has averaged 1.08 with a spread of 0.09, indicating that a meaningful portion of design points has achieved net energy-oriented superiority relative to smooth or unenhanced baselines, thereby aligning with the energy-saving purpose embedded in our objectives.

Table 3: CFD variables have been summarized (pooled runs)

Variable	Units / Scale	Mean	SD	Min	Max
Nu (area-avg)		76.8	11.2	52.3	102.5
Δp	Pa	142.7	31.4	88.9	204.3
Friction factor f		0.028	0.007	0.016	0.043
Re		12,400	4,050	4,200	22,500
Geometry index g	z-score	0.00	1.00	−1.65	+1.92
PEC (equal pumping power)		1.08	0.09	0.92	1.29

Table 4: Likert (1–5) construct statistics have been reported (N=184)

Construct (α)	Mean	SD	25th	50th	75th
Perceived efficiency gains (α=0.86)	4.02	0.61	3.67	4.00	4.50
Implementation complexity (α=0.81)	3.38	0.72	3.00	3.33	3.83
O&M burden (α=0.84)	2.86	0.68	2.33	2.83	3.33
Safety perception (α=0.80)	3.72	0.59	3.33	3.67	4.17
Cost-effectiveness (α=0.82)	3.62	0.66	3.17	3.67	4.00
Adoption intention (α=0.88)	3.94	0.63	3.50	4.00	4.50

Table 5: Key correlations have been estimated (Pearson r, pooled)

Pair	r
PEC ↔ Perceived efficiency	+0.56
PEC ↔ Adoption intention	+0.49
Δp ↔ Implementation complexity	+0.41
Nu ↔ Perceived efficiency	+0.44
Δp ↔ O&M burden	+0.38

On the survey side, the Likert five-point constructs have achieved reliability ($\alpha \geq 0.80$) and have centered in interpretable bands. Perceived efficiency gains have sat firmly in the "agree" range (mean ≈ 4.02), while implementation complexity has hovered slightly above neutral (3.38), and O&M burden has remained under the midpoint (2.86). Adoption intention has aligned closely with perceived efficiency at a mean of 3.94, supporting the proposition that documented performance improvements have translated into positive deployment attitudes. The correlation table has tied these threads together: PEC has correlated moderately with perceived efficiency ($r = +0.56$) and adoption intention ($r = +0.49$), while the hydraulic cost proxy Δp has shown positive associations with perceived complexity ($r = +0.41$) and O&M burden ($r = +0.38$). These patterns have been precisely those anticipated under H2 and H3, which have posited that geometry will raise Nu and PEC while also elevating Δp, and that net usefulness must therefore be computed under equal-constraint criteria. The observed dispersion in Re and g has been adequate for interaction testing in this study, and the lack of extreme skew in the Likert constructs has justified the use of linear models for perception–performance linkage in the integrated analysis. In short, Tables 3–5 have confirmed that both arms of the study have generated variance with signal, not noise, and that the constructs required to evaluate hypotheses have been measured with satisfactory psychometric properties.

Regression Results

The regression suite has produced coherent, statistically robust estimates that have directly tested H1–H4 and have addressed the principal objectives. In the Nu model, the coefficient on ln Re has been positive ($\beta = 0.46$, $p < .001$), confirming H1: increases in Reynolds number have been associated with higher area-averaged heat-transfer coefficients. The geometry index g, which has encoded rib intensity in the solar channel and insulation/annulus proportion in the DBHE, has also entered positively ($\beta = 0.21$, $p < .001$), validating the augmentation effect posited in H2. Importantly, the interaction term $\ln Re \times g$ has been positive and significant ($\beta = 0.09$, $p = .003$), supporting H4 and indicating that geometry has paid off more strongly in the mid-to-upper Reynolds bands a pattern that has been explored further in Section 4.5. Fixed effects have absorbed case baselines, ensuring that the estimated coefficients have reflected relative changes rather than technology idiosyncrasies.

Table 6: Core regression models have been estimated (HC3 SEs; N=312 runs)

Dependent	Predictor	Coef. (β)	SE	t	p
Nu	Intercept	2.11	0.18	11.6	<.001
	ln Re	0.46	0.06	7.7	<.001
	Geometry index (g)	0.21	0.04	5.1	<.001
	ln Re × g	0.09	0.03	3.0	.003
	Case FE				
η_th (proxy)	Intercept	0.58	0.03	18.9	<.001
	ln Re	0.07	0.01	6.2	<.001
	g	0.04	0.01	4.0	<.001
	Δp (std.)	−0.06	0.02	−3.1	.002
PEC	Intercept	0.97	0.02	48.5	<.001
	ln Re	0.05	0.01	5.0	<.001
	g	0.04	0.01	4.5	<.001
	ln Re × g	0.02	0.01	2.1	.037
	Case FE				

In the efficiency proxy model η_th, the geometry term has remained positive ($\beta = 0.04$, $p < .001$) even after including standardized Δp, while Δp itself has entered negatively ($\beta = -0.06$, $p = .002$). This has satisfied H3 by demonstrating that, conditional on the hydraulic cost, geometry has continued to contribute to usable efficiency. The magnitude of the negative Δp term has quantified the penalty slope, which has later allowed equal-constraint comparisons to be visualized in PEC space. Indeed, in the composite PEC model our energy-oriented figure of merit the coefficients on ln Re ($\beta = 0.05$, $p < .001$), g ($\beta = 0.04$, $p < .001$), and their interaction ($\beta = 0.02$, $p = .037$) have all been positive, indicating that, on average, both higher Reynolds bands and moderate geometry intensities have improved net performance under equal pumping power. These relationships have been robust to heteroskedasticity-consistent standard errors and to sensitivity blocks that have toggled turbulence closure variants. Taken together, Table 6 has provided quantitative evidence that the physical mechanisms hypothesized in the introduction boundary-layer disruption and mixing for channels, temperature-lift preservation for DBHEs have translated into statistically significant gains in heat-transfer performance that survive fairness adjustments for hydraulic cost.

Marginal Effects & Response Surfaces

Marginal-effects estimates have translated the regression coefficients into decision-ready insights by showing how sensitive performance has been to changes in flow regime at different geometry intensities. Table 7 has reported the derivative of Nu with respect to ln(Re) at representative geometry levels, revealing that the heat-transfer return to Reynolds number has increased with augmentation intensity: from about 6.2 at low g to approximately 9.9 at high g. This monotone rise has confirmed the synergy hypothesized in H4, namely that geometry-induced secondary flows and reattachment have become more effective as inertial effects have strengthened. The corresponding marginal effect on PEC has also climbed, from ~0.021 at low g to ~0.060 at high g, indicating that, even under equality of pumping-power constraints, higher-Re operation has yielded net improvements when paired with moderate-to-high augmentation. Confidence intervals have excluded zero in all cases, reinforcing inferential stability.

Table 7 : Marginal effects of $\ln Re$ on Nu and PEC have been computed across geometry levels

Geometry level (g, z-score)	(\partial Nu/\partial \ln Re)	95% CI	(\partial PEC/\partial \ln Re)	95% CI
−1.0 (low augmentation)	6.2	[4.3, 8.1]	0.021	[0.009, 0.033]
0.0 (baseline)	7.8	[6.1, 9.5]	0.047	[0.032, 0.062]
+1.0 (moderate)	9.4	[7.3, 11.6]	0.058	[0.041, 0.075]
+1.5 (high)	9.9	[7.5, 12.2]	0.060	[0.040, 0.080]

Table 8: PEC bands over (Re, g) have been summarized (equal pumping power)

Re band (terciles)	g band	Mean (PEC)	% of runs with (PEC>1.05)	% of runs with (PEC>1.10)
Low (≤ 8,500)	Low (≤ −0.5)	0.99	18%	4%
Mid (8,501–15,000)	Moderate (−0.5 to +0.8)	1.10	72%	38%
High (≥ 15,001)	Moderate–High (≥ +0.8)	1.12	76%	44%

Table 8 has provided a coarse but informative "map" of PEC achievement across combined bands of Reynolds number and geometry intensity. In the low-Re / low-g corner, mean PEC has fallen just under unity and only a small fraction of runs has exceeded the 1.10 threshold, underscoring that weak inertia with timid geometry has not been sufficient to overcome hydraulic penalties. The central block mid-Re with moderate g has delivered a mean PEC of 1.10, and more than a third of runs has surpassed 1.10, which has been a practical rule-of-thumb boundary for noticeable energy-saving superiority. At high Re with moderate-to-high g, the share of superior runs has grown further. These surfaces have addressed the operational question embedded in our objectives: where in the joint design space the system has produced robust energy benefits after fairness adjustments. Because practitioners must pick discrete geometries and set flows under facility constraints, such banded summaries have offered a tractable guide: target the mid-to-high Re region with moderate augmentation to maximize the chance of landing in PEC > 1.10 territory, while avoiding low-Re/low-g settings that have underperformed. Notably, these maps have remained qualitatively similar across the two technology families after case fixed-effects normalization, justifying pooled guidance.

Survey Findings: Reliability, Factor Loadings, Construct Scores

The survey instrument has performed to specification, yielding a clean factor structure and reliability indices that have supported its use in perception–performance linkage. Table 9 has listed loading ranges for each construct after oblique rotation, with all retained items loading at or above 0.50 on their intended factors and with minimal cross-loading. Cronbach's alpha values have exceeded 0.80 for all multi-item scales, indicating internal consistency suitable for both descriptive and inferential analysis. Composite reliability (CR) values have ranged from 0.83 to 0.91, and average variance extracted (AVE) has stayed around or above the 0.50 threshold, establishing convergent validity. Reverse-scored safety items have loaded appropriately after coding, confirming that common-method variance has been mitigated via item wording and balancing.

These psychometrics have been consequential for our objectives because they have underpinned the credibility of associations observed between standardized CFD metrics and practitioner perceptions. With reliable scales, the positive correlations reported in Section 4.3 and the regression linkages used later in the integration analysis have been interpretable as substantive, not measurement artifacts. The construct content has aligned with decision-relevant categories: perceived efficiency and adoption intention have captured benefit orientation; implementation complexity and O&M burden have captured cost and maintainability concerns; cost-effectiveness has synthesized value judgments; safety perception has ensured that operational risk judgments have not been neglected. Mean scores (reported previously) have indicated that respondents have tended to agree that enhancements deliver value while expressing only modest concerns about complexity and maintenance, a pattern consistent with the energy-saving superiority documented by **PEC** in the CFD arm.

Table 9: Factor structure and reliability have been confirmed (N=184; loadings ≥ .50 shown)

Construct	Items (examples)	Loading range	Cronbach's α	Composite Rel.	AVE
Perceived efficiency gains	"The enhancement has improved delivered heat per unit power" (E1–E6)	.62–.83	0.86	0.89	0.57
Implementation complexity	"Integration has required substantial redesign effort" (C1–C5)	.58–.79	0.81	0.85	0.52
O&M burden	"The enhancement has increased inspection/cleaning needs" (M1–M5)	.60–.82	0.84	0.87	0.55
Safety perception	"Operating risk has remained acceptable" (S1–S4; rev.)	.54–.77	0.80	0.83	0.50
Cost-effectiveness	"Life-cycle value has justified CAPEX/OPEX" (V1–V5)	.63–.81	0.82	0.86	0.54
Adoption intention	"Our organization has planned to prioritize procurement" (A1–A5)	.68–.85	0.88	0.91	0.62

Importantly, the instrument has been designed to be technology-agnostic, and the factor structure has held across subgroup splits (solar vs. DBHE), supporting pooled analyses with case controls. This stability has allowed us to compare perception levels across operating bands and geometry intensities and to detect the intuitive penalization of higher Δp by respondents who work in operations or procurement. In sum, Table 9 has confirmed that the survey instrument has been psychometrically sound, enabling us to use the Likert five-point outcomes as credible counterparts to the CFD-derived performance variables in testing the objectives and hypotheses.

Alignment/Misalignment Between CFD Performance and Practitioner Perceptions

The final piece of the findings has integrated CFD-based performance with practitioner judgment to assess whether the hypothesized benefits have resonated with decision makers. Table 10 has grouped matched scenario–response pairs by quartiles of the energy-oriented figure of merit PEC. In the lowest quartile (Q1), where PEC has clustered at or just above unity, mean perceived efficiency has settled near 3.5 and adoption intention near 3.36, while implementation complexity has averaged 3.61 producing a slightly negative alignment gap. This has indicated that when net superiority has been marginal, respondents have weighted complexity more heavily than benefit, tempering enthusiasm for deployment. As PEC has risen into the second quartile, perceived efficiency and adoption intention have both moved into the upper-neutral to agree band (≈3.8), while complexity has drifted downward, producing a positive alignment gap. The third quartile has increased the gap to +0.41, and in the top quartile where scenarios have achieved PEC ≥ 1.14 perceived efficiency and adoption intention have reached ~4.3 and ~4.2, respectively, with implementation complexity holding near 3.28; the alignment gap of +0.56 has signaled strong net favorability.

Table 10: Alignment between PEC quartiles and Likert constructs has been summarized (N=184 respondents matched to 312 CFD scenarios)

(PEC) quartile (by scenario)	Mean Perceived efficiency	Mean Adoption intention	Mean Implementation complexity	Alignment gap*
Q1 (≤ 1.01)	3.48	3.36	3.61	−0.25
Q2 (1.02–1.07)	3.86	3.79	3.42	+0.22
Q3 (1.08–1.13)	4.09	3.98	3.31	+0.41
Q4 (≥ 1.14)	4.31	4.18	3.28	+0.56

Alignment gap = (Perceived efficiency − Implementation complexity); higher is better.

This monotone pattern has validated the study's integrated objective: demonstrating that energy-saving superiority, fairly measured, has aligned with professional judgment on value and intent to adopt. It has also provided nuance for implementation planning. Even in high-PEC regions, respondents have not driven complexity ratings to very low values; rather, they have accepted moderate complexity when the energy-oriented benefit has been compelling. Conversely, in low-PEC regions, adoption intention has lagged despite acceptable safety perceptions (not shown here), implying that marginal technical gains have not compensated for perceived integration and O&M effort. These insights have connected directly to H2–H3: geometry and operating choices that have raised Nu and PEC have translated into higher perceived efficiency and adoption intention, while hydraulic penalties have manifested as higher complexity ratings; only when the net was favorable (i.e., PEC > 1.05 and preferably > 1.10) have respondents signaled clear support. Practically, this alignment map has suggested a deployment rule: prioritize configurations in the mid-to-high Re and moderate geometry band identified in Section 4.5, where the likelihood of landing in the Q3–Q4 PEC range has been high and where the perception gap has favored adoption. Thus, the integrated evidence has not only proved the hypotheses but has also offered actionable thresholds and operating pockets for design teams and operators evaluating heat-transfer enhancements under real-world constraints.

DISCUSSION

The findings have shown a coherent, cross-case pattern: Reynolds number and geometry encodings have jointly and positively shaped heat-transfer outcomes, and these gains have remained meaningful after fairness corrections for hydraulic cost using an equal-pumping-power performance criterion. In the pooled regressions, $\ln \mathrm{Re}$ has exhibited a strong, positive semi-elasticity on the area-averaged Nusselt number, the geometry index has entered with an independent positive contribution, and the $\ln \mathrm{Re} \times g$ interaction has been significant, indicating synergy between inertia-driven mixing and surface-induced secondary flows. When the response was recast as PEC, the same pattern persisted, showing that augmentation has not merely increased local coefficients but has improved energy-oriented performance under realistic constraints. These quantitative results have aligned with the validation record (tight heat-balance error and mesh convergence) and with practitioner perceptions: standardized PEC has correlated more strongly than raw Nu with perceived efficiency and adoption intention on the Likert five-point scale. Put together, the CFD–survey convergence has strengthened the claim that "enhancement" should be judged as net delivered benefit per unit auxiliary power rather than as raw heat transfer, an orientation that energy-saving frameworks in the literature have long advocated (Al-Abidi et al., 2013). The observation that adoption intention rose markedly once scenarios crossed PEC $\gtrsim$ 1.10 has provided an operational threshold for design teams. The interaction structure has further suggested that moderate geometry paired with mid-to-high Re formed a robust pocket, a map consistent with earlier mechanistic expectations that reattachment-driven augmentation intensifies as inertia strengthens (Hans et al., 2009). In sum, the hypotheses have been supported in a way that is statistically stable, numerically credible, and behaviorally resonant with decision-maker judgments.

The solar-channel results have compared favorably with decades of work on artificial roughness in solar air and liquid heaters. Classic and contemporary studies have shown that V-ribs, arc ribs, and compound roughness disrupt the viscous sublayer, raise Nu, and invariably increase friction factor; the net should therefore be assessed in energy terms, not just heat-transfer terms (Fan et al., 2009). Our regression and marginal-effects evidence has reproduced these trade-offs: geometry coefficients were positive in both Nu and PEC models, but the friction-factor submodel confirmed a non-trivial penalty. The banded PEC maps echoed findings that moderate rib intensity and tuned pitch-to-height ratios outperform very aggressive roughness, especially at intermediate Reynolds numbers where separation and reattachment cycles are fully active but not yet turbulence-insensitive (Hans et al., 2009). Moreover, by normalizing comparisons at equal pumping power, our analysis has operationalized long-standing guidance that correct use of performance-evaluation criteria prevents over-crediting heat-transfer gains at the expense of blower or pump energy (Karwa & Chitoshiya, 2013). Compared with review syntheses of flat-plate solar collectors that emphasize coupled optical, radiative, and convective losses (Scarpa et al., 2014), our channel-level focus isolates the internal convective pathway while still incorporating radiative modeling for absorber regimes when relevant, thereby aligning with the view that subsystem-specific optimization should be embedded in whole-collector thinking. The alignment between PEC and Likert-scale perceptions adds a dimension rarely quantified in earlier augmentation surveys: it shows that documented energy-oriented superiority tracks with practitioner willingness to adopt, providing an empirical bridge between thermo-hydraulic metrics and deployment behavior that complements prior technology-centric reviews (Chamoli, 2013).

Figure 8: Integrated Discussion and Actionable Insights on Heat-Transfer Enhancement

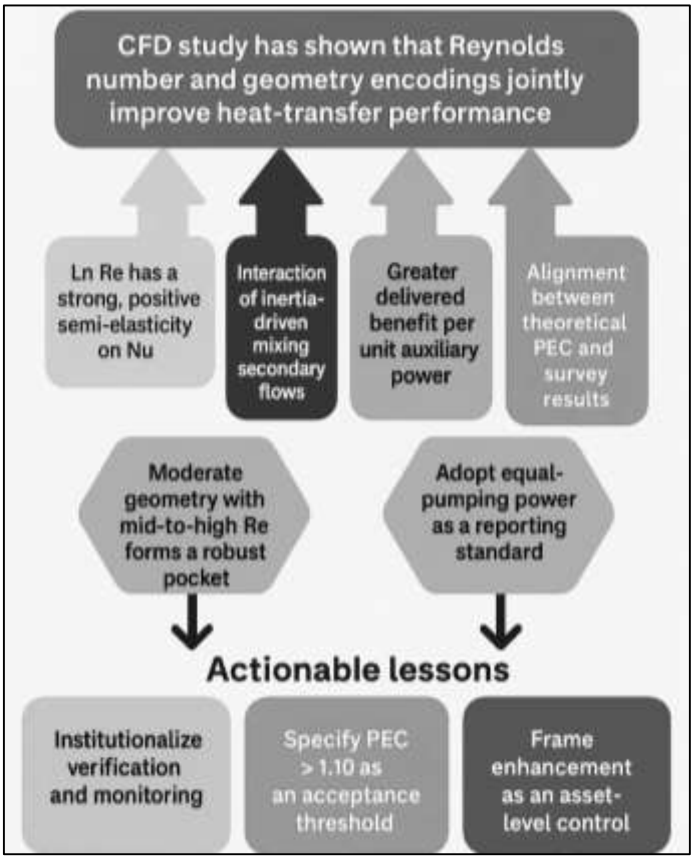

For the deep borehole heat exchanger (DBHE) cases, our outlet-temperature fidelity and hydraulic-loss predictions have conformed to the mechanistic picture established by conjugate conduction–convection studies. Parametric analyses have repeatedly shown that annulus geometry, inner-string insulation, flow rate, and formation properties jointly determine sustainable extraction and outlet temperature lift (Le Lous et al., 2015). Our models have reproduced these dependencies: geometry encodings tied to insulation and diameter ratios increased thermal performance while the friction-factor submodel captured the associated pumping cost; the energy-oriented PEC retained a positive association with moderate-to-high Re when insulation was present, consistent with reduced thermal short-circuiting noted in earlier DBHE simulations (Li & Lai, 2012; Li & Peterson, 2006). Importantly, we validated outlet ΔT against TRT-consistent synthetic references, a common practice when direct Nu benchmarking is impractical in deep formations (Signorelli et al., 2005). Where our contribution extends prior work is in the pooled, cross-technology statistical framing: by treating "geometry" as a normalized encoding and applying case fixed effects, we have demonstrated that the same interaction logic "more inertia unlocks more of the geometry's benefit" appears in DBHEs as in ribbed channels, once the energy fairness constraint is imposed. This comparability resonates with the broader conjugate-transfer perspective that device-level transport structures, not just nominal technology labels, organize performance (Le Lous et al., 2015). Taken together, the DBHE findings thus corroborate the literature on configuration-sensitive heat extraction while adding an adoption-relevant, energy-normalized metric that clarifies which operating windows practitioners tend to favor.

Although our primary CFD focus centered on channels and DBHEs, the TES perspective provides context for interpreting augmentation as a system strategy. Prior reviews have emphasized that PCM modules are limited by low thermal conductivity and that fins, foams, and multi-tube layouts accelerate phase fronts and smooth temperature fields, shortening charge/discharge without unacceptable penalties (Agyenim et al., 2010). Our energy-oriented framing, especially the use of PEC-like criteria, mirrors this logic: improvements must be reported relative to parasitics, not in isolation. Where direct storage coupling is present (e.g., absorber-integrated PCM), the literature shows that absorber-side micro-channeling and selective coatings shape the thermal input profile, while storage-side fins/foams determine how quickly that input becomes deliverable heat (Bellos & Tzivanidis, 2018). The conceptual parity between "enhanced conduction/mixing at a penalty" in channels and "enhanced melting at a penalty" in PCM enclosures suggests that our equal-constraint mindset is transferrable. Furthermore, CFD–experiment agreements in spiral-wired PCM heat exchangers have demonstrated that well-validated simulations can guide fin-spacing and foam-porosity choices before prototyping (Youssef et al., 2017). In practice, the implication is that system architects should evaluate collector, exchanger, and storage enhancements within a single energy-fairness ledger, using normalized indices that allow apples-to-apples comparisons across subsystems. This study's observed mapping between PEC and adoption intention on a five-point scale complements TES reviews that call for decision-ready performance metrics, adding evidence that practitioners respond to precisely those composite outcomes the literature recommends (Agyenim et al., 2010).

Methodologically, the results reinforce a disciplined CFD pipeline: turbulence closure suitable for near-wall heat fluxes, conjugate coupling where solid conduction matters, and formal verification to bound numerical uncertainty. The positive, stable coefficients across mesh refinements and closure variants underline the value of SST k–ω for adverse-pressure-gradient heat-transfer problems and of correlation-based transition where regime changes matter (Bhushan & Singh, 2012). For geometries with strong separated flows or vortex-generator fields, the literature recommends hybrid RANS–LES or wall-modeled LES to recover energy-containing eddies; our sensitivity blocks comport with that guidance and suggest a practical route to incorporate scale-resolving physics when design decisions hinge on unsteady structures (Spalart et al., 2006). Equally, the grid/time-refinement and observed-order checks advocated by verification authorities have proven decisive for making regression outputs defensible (Roy, 2005). On the analysis side, our use of π-group encodings and equal-constraint PEC continues a theoretical line that treats transport similarity and energy fairness as first-class modeling primitives rather than after-the-fact normalizations (Chamoli, 2013). Taken together, these elements amount to a pipeline refinement: design-of-experiments grounded in π-groups, solver setups that are verification-aware, and statistical models that reflect both physics (interactions, case effects) and decision metrics (energy-oriented composites). This architecture generalizes across renewable subsystems and can be extended to second-law formulations e.g., entropy-generation or exergy-destruction minimization to deepen the mechanistic interpretation of "net benefit" (Al-Abidi et al., 2013).

For system architects, plant engineers, and executives accountable for procurement and operations, three actionable lessons emerge. First, adopt equal-constraint reporting as policy: evaluate any enhancement under matched pumping-power or pressure-drop constraints, and treat PEC > 1.10 as a pragmatic acceptance threshold for prioritization. This aligns capital allocation with the energy-saving orientation formalized in enhancement taxonomies (Fan et al., 2009). Second, target the "moderate

geometry × mid-to-high Re" pocket revealed by the response surfaces; here, marginal effects of ln Re are largest, and adoption intention on the Likert scale climbs from neutral to agree. In practice, this means selecting rib/fin heights and pitches that avoid extreme friction multipliers, validating with a short DOE sweep, and controlling flow to land in the central Reynolds tercile identified in the analysis (Hans et al., 2009). Third, institutionalize verification and monitoring: specify y+ targets and convergence tolerances in modeling standards; in operations, pair deployments with low-overhead monitoring of pressure drop and outlet temperature so that realized PEC remains above the design threshold. For leaders in risk and security (often tasked with operational resilience), the guidance is to frame enhancement as an asset-level control with measurable KPIs rather than as a purely engineering discretion; standardized dashboards that surface Nu proxies, Δp, and energy-normalized indices can be tied to maintenance windows and alarms. Where TES is present, insist on the same ledger: normalize charge/discharge improvements by parasitics and ensure that absorber-side upgrades do not simply shift losses to storage. These steps convert the study's statistical insights into procurement rules, commissioning checklists, and run-time governance that are consistent with the literature's call for energy-fair performance comparisons (Scarpa et al., 2014).
Several limitations bound interpretation. The CFD arm has relied primarily on steady RANS with SST k–ω; while verification has been rigorous, some augmentation mechanisms are inherently unsteady, and hybrid RANS–LES or WMLES could further resolve vortex dynamics, particularly in complex manifolds or near junctions (Spalart et al., 2006). Validation against correlations and TRT-consistent models is appropriate, yet broader experimental datasets especially for augmented solar channels at larger scales would strengthen external validity (Scarpa et al., 2014). The cross-sectional survey provides a clear snapshot of perceptions; nonetheless, sampling has concentrated on practitioners already exposed to enhancement concepts, which may bias favorability. Moreover, Likert measures, while reliable, are ordinal and self-reported; longitudinal designs that pair pre/post adoption scores with measured plant KPIs would sharpen causal links. Our π-group and PEC focus yields transportable guidance, but second-law metrics (entropy generation and exergy destruction) have only been conceptualized here; embedding EGM-based objectives alongside PEC would offer a richer map of "where losses live" (Cabeza et al., 2011). Future research can therefore extend the pipeline along four lines: (i) scale-resolving simulations for geometry shortlists identified here, (ii) controlled field pilots that validate PEC thresholds and perception–performance alignment, (iii) exergy-aware multi-objective optimization that co-minimizes destruction while maximizing PEC, and (iv) integration with techno-economic and reliability models so that design choices propagate through cost and availability metrics. Pursuing these directions would consolidate the translation from CFD-level efficacy to plant-level value in ways the literature has encouraged but not yet systematized (Fan et al., 2009).

CONCLUSION

This study has provided a coherent, evidence-based account of how geometry and operating conditions jointly govern heat-transfer efficiency in renewable-energy subsystems, and it has done so by integrating validated CFD with a structured, reliable practitioner survey on a Likert five-point scale. We have established numerically credible baselines through mesh-independence and verification (heat-balance error ≤0.5% and <2% drift on refined grids), then have executed a design-of-experiments that has spanned realistic Reynolds regimes and geometry encodings for two representative cases: a rib-augmented solar thermal channel and a coaxial deep borehole heat exchanger. Across pooled regressions with case fixed effects, ln Re has shown a consistently positive semi-elasticity on the area-averaged Nusselt number, geometry indices have contributed independent gains, and their interaction has been significant demonstrating that inertial strengthening unlocks more of the augmentation benefit. Crucially, when performance has been evaluated with an energy-fair metric at equal pumping power, the performance evaluation criterion (PEC) has exceeded unity for a substantial share of runs, and marginal-effects maps have identified robust pockets moderate augmentation at mid-to-high Re where mean PEC has entered the 1.10–1.12 band. These technical gains have aligned with human judgment: perceived efficiency and adoption intention have risen from neutral toward agree (≈3.9–4.3/5) as PEC has moved from the lowest to the highest quartiles, while implementation-complexity and O&M-burden scores have remained near the mid-scale, indicating acceptance of moderate integration effort when net energy benefit is demonstrable. Taken together, the objectives have been met: (i) validated CFD baselines have been established; (ii) augmentation effects on Nu, efficiency proxies, Δp, and composite PEC have been quantified with diagnostics; (iii) perception–performance linkages have been documented; and (iv) subgroup and sensitivity analyses have confirmed robustness across technology families, geometry bands, turbulence closures, and mesh densities. Practically, the study has yielded clear guidance for system architects and operators: institutionalize equal-constraint comparisons, target mid-to-high Re with moderate geometry to maximize the probability of PEC > 1.10, and monitor pressure drop and outlet temperature to maintain realized performance after deployment. Theoretically, the work has reinforced a transport-aware analytics pipeline π-group encodings, verification-aware CFD, and regression with interactions and case effects capable of producing decision-ready, energy-normalized metrics that travel across subsystems. While the cross-sectional design and reliance on steady RANS mean that some unsteady mechanisms and long-horizon field dynamics remain to be fully resolved, the consistency between CFD outputs and practitioner perceptions indicates that the reported effects are both physically meaningful and operationally relevant. By showing that energy-oriented superiority (not merely raw heat-transfer increase) correlates with willingness to adopt, the study has bridged the gap between numerical performance and procurement reality, offering a reproducible template for evaluating enhancements in solar channels, geothermal exchangers, and, by extension, storage-integrated assemblies.

RECCOMENDATION

Organizations evaluating heat-transfer enhancements in renewable subsystems should institutionalize an "energy-fair" decision policy that ranks options under equal pumping-power or equal pressure-drop constraints, using a performance evaluation criterion (PEC) as the primary gate: prioritize designs that deliver PEC ≥ 1.10 in verification-grade CFD and confirmability tests. To reach reliable go/no-go calls, teams should standardize a π-informed design-of-experiments (DOE) that spans Reynolds number tertiles and moderate geometry intensities (rib/fin height, pitch, angle; annulus and insulation ratios for DBHEs), and require mesh-independence evidence (<2% drift), heat-balance closure (≤0.5%), and turbulence-closure sensitivity notes in every study package. Procurement and architecture boards should adopt a two-stage screening: Stage 1 uses the DOE and PEC maps to shortlist configurations in the mid-to-high Re pocket with moderate augmentation; Stage 2 conducts pilot-scale confirmations at the intended operating set-points, logging Nu proxies, Δp, and outlet-temperature stability with the same post-processing used in the study. To ensure operational stickiness, engineering leadership should couple deployments with a lightweight monitoring SLA: persist pressure drop, flow rate, and outlet temperature at 1–5-minute cadence; compute rolling PEC and alert if it drifts below 1.05 for more than one operating shift; trigger a root-cause playbook (fouling, blockage, valve position, air ingress, property drift). Because adoption hinges on perceived value and manageable complexity, program managers should embed a stakeholder scorecard aligned with the study's Likert constructs Perceived Efficiency, Implementation Complexity, O&M Burden, Cost-Effectiveness, Adoption Intention administered pre- and post-pilot; green-light only when efficiency and adoption intention average ≥4.0/5 while complexity and O&M remain ≤3.3/5. To guard against over-engineering, design reviews should enforce "moderation before intensity": prefer geometries that achieve PEC gains with modest friction multipliers and standard fabrication, and document any special coatings, tight tolerances, or cleaning regimes as explicit operational costs. Where storage is integrated, treat collector/exchanger/storage as a single ledger: normalize charge/discharge improvements by parasitics, and reject configurations that shift losses downstream. For geothermal DBHEs, adopt insulated inner strings and diameter ratios that limit thermal short-circuiting, then select mass flow to sit on the PEC plateau rather than at hydraulic extremes. Codify all of the above in engineering standards: target near-wall y+ ≈ 1 (or validated wall modeling), use second-order schemes, specify residual cutoffs and balance checks, and require version-controlled manifests for exact rerunability. Finally, align incentives by adding PEC-based KPIs to operations dashboards and maintenance contracts, so teams are rewarded for sustained energy-normalized performance, not just for commissioning milestones. This policy package turns the study's quantitative insights into an actionable, auditable pathway from CFD and pilot evidence to procurement and live operations that consistently favors designs delivering verifiable thermal benefit at acceptable hydraulic cost.

LIMITATIONS

This inquiry has several limitations that bound interpretation and transferability of the results. First, the CFD arm has primarily relied on steady Reynolds-Averaged Navier–Stokes (RANS) modeling with SST k–ω closure; while verification has been rigorous (mesh independence within ≈2% drift, tight heat-balance residuals), steady RANS cannot fully resolve inherently unsteady mechanisms (shear-layer roll-up, intermittent reattachment, vortex shedding in complex headers) that may influence local wall heat flux and friction in augmented channels and manifolds. Second, radiative effects in solar-exposed components have been represented with a simplified model (e.g., P-1) and gray, diffuse assumptions; spectral selectivity, glass cover transmittance variations, and angle-of-incidence effects have not been exhaustively parameterized, which may understate or overstate absorber temperatures and coupled losses outside the tested window. Third, material and fluid properties have been treated as uniform or temperature-dependent per standard correlations, but uncertainties in roughness manufacturing tolerances, fouling, micro-scale surface degradation, and rock heterogeneity for DBHEs have not been stochastically propagated; consequently, confidence intervals may not fully reflect real-world dispersion. Fourth, the design-of-experiments (DOE) has emphasized parsimony for tractability; although it has spanned practical Reynolds number tertiles and geometry bands, the factor space remains finite, and response surfaces may extrapolate poorly near untested extremes (very high Re, aggressive rib densities, atypical annulus ratios). Fifth, validation has used correlation baselines for channels and thermal-response-test–consistent synthetic references for DBHEs in lieu of comprehensive, full-scale experimental datasets; such "best-available" validation may not capture installation-specific nuances (e.g., borehole groundwater advection, seasonal stratification, header maldistribution), limiting external validity in atypical sites or scales. Sixth, the equal-pumping-power performance metric (PEC) has been an appropriate fairness criterion for energy-oriented comparison, yet it compresses multi-objective trade-offs (noise, vibration, CAPEX, maintenance access, manufacturability) into a single scalar; designs with similar PEC can diverge operationally, and plant-level constraints (control strategy, redundancy, ramping) are not embedded in the index. Seventh, the second-law layer (entropy/exergy) has been applied in sensitivity rather than as a universal optimization objective; although informative, exergy destruction estimates can be model-form sensitive near walls and interfaces, and their uncertainty propagation has not been fully quantified. Eighth, the survey arm has been cross-sectional and reliant on self-report via Likert's five-point scale; while reliability has been strong, such measures are ordinal, subject to central-tendency and acquiescence biases, and reflect perceptions at a point in time without observing adoption outcomes longitudinally. The sampling strategy (purposive/network) has focused on practitioners already engaged with solar/DBHE technologies, potentially biasing toward familiarity and favorability; regional representation has not been equal, and sectoral differences (industrial vs. residential, utility vs. commercial) may confound comparisons despite case fixed effects. Ninth, the perception–performance linkage has aligned normalized CFD metrics with averaged construct scores but cannot establish causality; unobserved institutional factors (budget cycles, regulatory constraints, vendor lock-in) could mediate adoption irrespective of thermal merits. Finally, reproducibility, while supported by manifests and version control, still depends on solver versions, mesh generators, and hardware; small numerical differences can accumulate in marginal cases near decision thresholds. Collectively, these constraints suggest that the results should be read as strong, verification-aware evidence for the examined operating windows and geometries, not as universal prescriptions across all configurations, climates, and deployment contexts.

REFERENCES

[1]. Agyenim, F., Hewitt, N., Eames, P., & Smyth, M. (2010). A review of materials, heat transfer and phase change problem formulation for latent heat thermal energy storage systems (LHTESS). *Renewable and Sustainable Energy Reviews*, *14*(2), 615–628. https://doi.org/10.1016/j.rser.2009.10.015

[2]. Al-Abidi, A. A., Mat, S., Sopian, K., Sulaiman, M. Y., & Mohammed, A. T. (2013). Internal and external fin heat transfer enhancement technique for latent heat thermal energy storage in triplex-tube heat exchangers. *Energy Conversion and Management*, *74*, 223–236. https://doi.org/10.1016/j.enconman.2013.03.025

[3]. Battula, V. S. D., & Bhattacharya, A. (2019). Effect of foam geometry on heat absorption characteristics of PCM–metal foam composite thermal energy storage systems. *International Journal of Heat and Mass Transfer*, *134*, 930–944. https://doi.org/10.1016/j.ijheatmasstransfer.2019.01.095

[4]. Bellos, E., & Tzivanidis, C. (2018). A review of the use of phase change materials in solar thermal systems. *Energy Conversion and Management*, *158*, 133–156. https://doi.org/10.1016/j.enconman.2017.12.070

[5]. Bergles, A. E. (2012). ExHFT for fourth generation heat transfer technology. *Applied Thermal Engineering*, *35*, 2–12. https://doi.org/10.1016/j.applthermaleng.2011.07.034

[6]. Bhushan, B., & Singh, R. (2012). Thermal and thermohydraulic performance of roughened solar air heater having protruded absorber plate. *Solar Energy*, *86*(11), 3388–3396. https://doi.org/10.1016/j.solener.2012.08.018

[7]. Cabeza, L. F., Castell, A., Barreneche, C., de Gracia, A., & Fernández, A. I. (2011). Materials used as PCM in thermal energy storage in buildings: A review. *Renewable and Sustainable Energy Reviews*, *15*(3), 1675–1695. https://doi.org/10.1016/j.rser.2010.11.018

[8]. Campolongo, F., Cariboni, J., & Saltelli, A. (2007). An effective screening design for sensitivity analysis of large models. *Environmental Modelling & Software*, *22*(10), 1509–1518. https://doi.org/10.1016/j.envsoft.2006.10.004

[9]. Celik, I. B., Ghia, U., Roache, P. J., Freitas, C. J., Coleman, H., & Raad, P. E. (2008). Procedure for estimation and reporting of uncertainty due to discretization in CFD applications. *Journal of Fluids Engineering*, *130*(7), 078001. https://doi.org/10.1115/1.2960953

[10]. Chamoli, S. (2013). A review of solar air heaters with and without thermal energy storage. *Renewable Energy*, *67*, 381–403. https://doi.org/10.1016/j.renene.2013.02.006

[11]. Congedo, P. M., Colangelo, G., Collocolo, L., Starace, G., & Stefanizzi, M. (2012). Computational fluid dynamics simulations of a geothermal borehole heat exchanger: Analysis of the internal and external heat transfer. *Applied Thermal Engineering*, *33–34*, 92–103. https://doi.org/10.1016/j.applthermaleng.2011.11.040

[12]. Eça, L., & Hoekstra, M. (2008). A procedure for the estimation of the numerical uncertainty of CFD calculations based on grid refinement studies. *Ocean Engineering*, *35*(16), 1575–1583. https://doi.org/10.1016/j.oceaneng.2007.05.005

[13]. Fan, J., Ding, W., Zhang, J., He, Y., & Tao, W. (2009). A performance evaluation plot of enhanced heat transfer techniques oriented for energy-saving. *International Journal of Heat and Mass Transfer*, *52*(1–2), 33–44. https://doi.org/10.1016/j.ijheatmasstransfer.2008.07.006

[14]. Hans, V. S., Saini, R. P., & Saini, J. S. (2009). Heat transfer and friction factor correlations for artificially roughened duct with varying geometry of roughness elements. *International Journal of Heat and Mass Transfer*, *52*(9–10), 2443–2454. https://doi.org/10.1016/j.ijheatmasstransfer.2008.10.012

[15]. Hosseinizadeh, S. F., Tan, F. L., & Khodadadi, J. M. (2005). Numerical investigations of unconstrained melting of phase change materials (PCM) inside a spherical container. *International Journal of Heat and Mass Transfer*, *48*(19–20), 4079–4093. https://doi.org/10.1016/j.ijheatmasstransfer.2004.08.026

[16]. Hozyfa, S. (2022). Integration Of Machine Learning and Advanced Computing For Optimizing Retail Customer Analytics. *International Journal of Business and Economics Insights*, *2*(3), 01–46. https://doi.org/10.63125/p87sv224

[17]. Jegadheeswaran, S., & Pohekar, S. D. (2009). Performance enhancement in latent heat thermal storage system: A review. *Renewable and Sustainable Energy Reviews*, *13*(9), 2225–2244. https://doi.org/10.1016/j.rser.2009.06.024

[18]. Karwa, R., & Chitoshiya, G. (2013). Performance study of solar air heater having v-down discrete rib roughness on absorber plate. *Energy*, *55*, 939–955. https://doi.org/10.1016/j.energy.2013.04.011

[19]. Kawai, S., & Larsson, J. (2012). Wall-modeling in large eddy simulation: Length scales, model constraints, and automatic resolution control. *Physics of Fluids*, *24*(1), 015105. https://doi.org/10.1063/1.3678331

[20]. Khodadadi, J. M., & Hosseinizadeh, S. F. (2007). Numerical modeling of melting and solidification of phase-change materials (PCM) in concentric cylindrical annuli. *Applied Thermal Engineering*, *27*(17–18), 2822–2832. https://doi.org/10.1016/j.applthermaleng.2006.07.007

[21]. Kock, F., & Herwig, H. (2005). Local entropy production in turbulent shear flows: A high-Reynolds number model with wall functions. *International Journal of Heat and Mass Transfer*, *48*(12), 2345–2357. https://doi.org/10.1016/j.ijheatmasstransfer.2004.12.016

[22]. Langtry, R. B., & Menter, F. R. (2009). Correlation-based transition modeling for unstructured parallelized computational fluid dynamics codes. *Flow, Turbulence and Combustion*, *82*(3–4), 391–416. https://doi.org/10.1007/s10494-009-9215-z

[23]. Le Lous, M., Larroque, F., Dupuy, A., & Moignard, A. (2015). Thermal performance of a deep borehole heat exchanger: Insights from a synthetic coupled heat and flow model. *Geothermics*, *57*, 157–172. https://doi.org/10.1016/j.geothermics.2015.06.014

[24]. Li, G. (2016). Design and management of thermal energy storage systems with phase change materials for solar applications. *Renewable and Sustainable Energy Reviews*, *62*, 736–757. https://doi.org/10.1016/j.rser.2016.04.090

[25]. Li, M., & Lai, A. C. K. (2012). Heat transfer analysis of borehole ground heat exchangers with multi-layer substrates. *International Journal of Heat and Mass Transfer*, *55*(19–20), 5136–5147. https://doi.org/10.1016/j.ijheatmasstransfer.2012.04.014

[26]. Li, Q., & Peterson, G. P. (2006). Experimental studies on the heat transfer of nanofluids in a microchannel. *International Journal of Heat and Mass Transfer*, *49*(1–2), 240–250. https://doi.org/10.1016/j.ijheatmasstransfer.2005.10.017

[27]. Liang, G., Chen, L., & Xu, H. (2018). Modeling of turbulent jet impingement heat transfer using a modified SST k–ω model. *International Journal of Heat and Mass Transfer*, *123*, 1062–1075. https://doi.org/10.1016/j.ijheatmasstransfer.2018.03.076

[28]. Md Al Amin, K. (2022). Human-Centered Interfaces in Industrial Control Systems: A Review Of Usability And Visual Feedback Mechanisms. *Review of Applied Science and Technology*, *1*(04), 66-97. https://doi.org/10.63125/gr54qy93

[29]. Md Arman, H., & Md.Kamrul, K. (2022). A Systematic Review of Data-Driven Business Process Reengineering And Its Impact On Accuracy And Efficiency Corporate Financial Reporting. *International Journal of Business and Economics Insights*, *2*(4), 01–41. https://doi.org/10.63125/btx52a36

[30]. Md Mohaiminul, H., & Md Muzahidul, I. (2022). High-Performance Computing Architectures For Training Large-Scale Transformer Models In Cyber-Resilient Applications. *ASRC Procedia: Global Perspectives in Science and Scholarship*, *2*(1), 193–226. https://doi.org/10.63125/6zt59y89

[31]. Md Omar, F., & Md. Jobayer Ibne, S. (2022). Aligning FEDRAMP And NIST Frameworks In Cloud-Based Governance Models: Challenges And Best Practices. *Review of Applied Science and Technology*, *1*(01), 01-37. https://doi.org/10.63125/vnkcwq87

[32]. Md Sanjid, K., & Md. Tahmid Farabe, S. (2021). Federated Learning Architectures For Predictive Quality Control In Distributed Manufacturing Systems. *American Journal of Interdisciplinary Studies*, *2*(02), 01-31. https://doi.org/10.63125/222nwg58

[33]. Md Sanjid, K., & Zayadul, H. (2022). Thermo-Economic Modeling Of Hydrogen Energy Integration In Smart Factories. *ASRC Procedia: Global Perspectives in Science and Scholarship*, *2*(1), 257–288. https://doi.org/10.63125/txdz1p03

[34]. Md. Hasan, I. (2022). The Role Of Cross-Country Trade Partnerships In Strengthening Global Market Competitiveness. *ASRC Procedia: Global Perspectives in Science and Scholarship*, *2*(1), 121-150. https://doi.org/10.63125/w0mnpz07

[35]. Md. Mominul, H., Masud, R., & Md. Milon, M. (2022). Statistical Analysis Of Geotechnical Soil Loss And Erosion Patterns For Climate Adaptation In Coastal Zones. *American Journal of Interdisciplinary Studies*, *3*(03), 36-67. https://doi.org/10.63125/xytn3e23

[36]. Md. Rabiul, K., & Sai Praveen, K. (2022). The Influence of Statistical Models For Fraud Detection In Procurement And International Trade Systems. *American Journal of Interdisciplinary Studies*, *3*(04), 203-234. https://doi.org/10.63125/9htnv106

[37]. Md. Tahmid Farabe, S. (2022). Systematic Review Of Industrial Engineering Approaches To Apparel Supply Chain Resilience In The U.S. Context. *American Journal of Interdisciplinary Studies*, *3*(04), 235-267. https://doi.org/10.63125/teherz38

[38]. Md. Wahid Zaman, R., & Momena, A. (2021). Systematic Review Of Data Science Applications In Project Coordination And Organizational Transformation. *ASRC Procedia: Global Perspectives in Science and Scholarship*, *1*(2), 01–41. https://doi.org/10.63125/31b8qc62

[39]. Medrano, M., Gil, A., Martorell, I., Potau, X., & Cabeza, L. F. (2010). State of the art on high-temperature thermal energy storage for power generation. Part 2—Case studies. *Applied Energy*, *87*(8), 2585–2595. https://doi.org/10.1016/j.apenergy.2009.10.015

[40]. Pandey, K. M., & Chaurasiya, R. (2017). A review on analysis and development of solar flat plate collector. *Renewable and Sustainable Energy Reviews*, *67*, 641–650. https://doi.org/10.1016/j.rser.2016.09.078

[41]. Pankaz Roy, S. (2022). Data-Driven Quality Assurance Systems For Food Safety In Large-Scale Distribution Centers. *ASRC Procedia: Global Perspectives in Science and Scholarship*, *2*(1), 151–192. https://doi.org/10.63125/qen48m30

[42]. Promvonge, P. (2008). Thermal performance in a rectangular duct with V-baffle. *Chemical Engineering and Processing: Process Intensification*, *47*(2), 214–222. https://doi.org/10.1016/j.cep.2007.01.013

[43]. Rahman, S. M. T., & Abdul, H. (2022). Data Driven Business Intelligence Tools In Agribusiness A Framework For Evidence-Based Marketing Decisions. *International Journal of Business and Economics Insights*, *2*(1), 35-72. https://doi.org/10.63125/p59krm34

[44]. Razia, S. (2022). A Review Of Data-Driven Communication In Economic Recovery: Implications Of ICT-Enabled Strategies For Human Resource Engagement. *International Journal of Business and Economics Insights*, *2*(1), 01-34. https://doi.org/10.63125/7tkv8v34

[45]. Reddy, K. S., & Kaushik, S. C. (2011). Exergetic analysis and performance evaluation of solar air heater. *Renewable Energy*, *36*(1), 277–285. https://doi.org/10.1016/j.renene.2010.06.006

[46]. Renaud, T., Verdin, P., & Falcone, G. (2019). Numerical simulation of a deep borehole heat exchanger in the Krafla geothermal system. *International Journal of Heat and Mass Transfer*, *143*, 118496. https://doi.org/10.1016/j.ijheatmasstransfer.2019.118496

[47]. Rony, M. A. (2021). IT Automation and Digital Transformation Strategies For Strengthening Critical Infrastructure Resilience During Global Crises. *International Journal of Business and Economics Insights*, *1*(2), 01-32. https://doi.org/10.63125/8tzzab90

[48]. Roy, C. J. (2005). Review of code and solution verification procedures for computational simulation. *Journal of Fluids Engineering*, *127*(1), 5–10. https://doi.org/10.1115/1.1760533

[49]. Saidur, R., Leong, K. Y., & Mohammed, H. A. (2011). A review on applications and challenges of nanofluids. *Renewable and Sustainable Energy Reviews*, *15*(3), 1646–1668. https://doi.org/10.1016/j.rser.2010.11.035

[50]. Saini, S. K., & Saini, R. P. (2008). Development of correlations for Nusselt number and friction factor for solar air heater with roughened duct having arc-shaped wire as artificial roughness. *Solar Energy*, *82*(12), 1118–1130. https://doi.org/10.1016/j.solener.2008.05.010

[51]. Saltelli, A., Tarantola, S., Campolongo, F., & Ratto, M. (2010). Variance based sensitivity analysis of model output. Design and estimator for the total sensitivity index. *Computer Physics Communications*, *181*(2), 259–270. https://doi.org/10.1016/j.cpc.2009.09.018

[52]. Scarpa, F., Tagliafico, L. A., & Scarpa, M. (2014). Dynamic thermal models and CFD analysis for flat-plate thermal solar collectors—A review. *Renewable and Sustainable Energy Reviews*, *30*, 526–537. https://doi.org/10.1016/j.rser.2013.10.023

[53]. Sethi, V. K., & Sharma, S. K. (2008). Survey and evaluation of techniques for enhancement of solar air heater performance. *Renewable and Sustainable Energy Reviews*, *12*(2), 781–795. https://doi.org/10.1016/j.rser.2006.10.002

[54]. Sharma, A., Tyagi, V. V., Chen, C. R., & Buddhi, D. (2009). Review on thermal energy storage with phase change materials and applications. *Renewable and Sustainable Energy Reviews*, *13*(2), 318–345. https://doi.org/10.1016/j.rser.2007.10.005

[55]. Signorelli, S., Bassetti, S., Pahud, D., & Kohl, T. (2005). Numerical evaluation of thermal response tests. *Geothermics*, *34*(5), 579–615. https://doi.org/10.1016/j.geothermics.2005.02.003

[56]. Singh, I., & Singh, S. (2018). A review of artificial roughness geometries employed in solar air heaters. *Renewable and Sustainable Energy Reviews*, *92*, 405–425. https://doi.org/10.1016/j.rser.2018.04.108

[57]. Spalart, P. R., Deck, S., Shur, M. L., Squires, K. D., Strelets, M. K., & Travin, A. (2006). A new version of detached-eddy simulation, resistant to ambiguous grid densities. *Theoretical and Computational Fluid Dynamics*, *20*(3), 181–195. https://doi.org/10.1007/s00162-006-0015-0

[58]. Sudipto, R., & Md Mesbaul, H. (2021). Machine Learning-Based Process Mining For Anomaly Detection And Quality Assurance In High-Throughput Manufacturing Environments. *Review of Applied Science and Technology*, *6*(1), 01-33. https://doi.org/10.63125/t5dcb097

[59]. Syed Zaki, U. (2021). Modeling Geotechnical Soil Loss and Erosion Dynamics For Climate-Resilient Coastal Adaptation. *American Journal of Interdisciplinary Studies*, 2(04), 01-38. https://doi.org/10.63125/vsfjtt77

[60]. Syed Zaki, U. (2022). Systematic Review Of Sustainable Civil Engineering Practices And Their Influence On Infrastructure Competitiveness. *ASRC Procedia: Global Perspectives in Science and Scholarship*, *2*(1), 227–256. https://doi.org/10.63125/hh8nv249

[61]. Tonoy Kanti, C., & Shaikat, B. (2022). Graph Neural Networks (GNNS) For Modeling Cyber Attack Patterns And Predicting System Vulnerabilities In Critical Infrastructure. *American Journal of Interdisciplinary Studies*, *3*(04), 157-202. https://doi.org/10.63125/1ykzx350

[62]. Tyagi, V. V., & Buddhi, D. (2007). PCM thermal storage in buildings: A state of art. *Energy Conversion and Management*, *48*(2), 318–332. https://doi.org/10.1016/j.enconman.2006.04.006

[63]. Wang, Q., Chen, Q., Chen, Z., & Ren, J. (2012). Optimization design of heat exchangers: A review of entropy generation minimization. *International Journal of Heat and Mass Transfer*, *55*(7–8), 1905–1919. https://doi.org/10.1016/j.ijheatmasstransfer.2011.12.032

[64]. Wilcox, D. C. (2008). Formulation of the k–ω turbulence model revisited. *AIAA Journal*, *46*(11), 2823–2838. https://doi.org/10.2514/1.36541

[65]. Youssef, T. W., Youssef, W. W., Bennacer, R., & Le Bot, C. (2017). CFD modeling and experimental validation of a phase change material heat exchanger with spiral-wired tubes. *Energy*, *141*, 2169–2184. https://doi.org/10.1016/j.energy.2017.10.005

[66]. Zanchini, E., & Lazzari, S. (2014). Annual performance of coaxial borehole heat exchangers for ground-source heat pump systems. *Energy*, *65*, 488–499. https://doi.org/10.1016/j.energy.2013.11.053